

# Non-equilibrium Hadrochemistry in QGP Hadronization

Johann Rafelski\* and Jean Letessier<sup>†</sup>

*\*Department of Physics, University of Arizona, Tucson, AZ, 85721*

*<sup>†</sup>Laboratoire de Physique Théorique et Hautes Energies  
Université Paris 7, 2 place Jussieu, F-75251 Cedex 05*

**Abstract.** This survey offers an introductory tutorial for students of any age of the currently thriving field of hadrochemistry. We discuss the different chemical potentials, how the hadronic phase space is described and how one evaluates the abundance of hadrons at time of hadronization. We show that a rather accurate description of experimental data arises and we present results of fits to hadron yields at SPS and RHIC. We show that introduction of chemical non-equilibrium originating in a sudden hadronization of a QGP is favored strongly at SPS and is presently also emerging at RHIC. The low chemical freeze-out temperatures are consistent with the picture of single freeze-out scenario (chemical and thermal freeze-out coincide).

## 1. THERMAL EQUILIBRIUM

Hadronic interactions are strong, collisions are frequent, and along with Hagedorn [1, 2, 3], we expect formation of statistical equilibrium conditions. The formation of a space-time-localized fireball of dense matter is the key physical process occurring in high energy nuclear collisions. This said, the question is how such a fireball can possibly arise from a rather short sequence of individual reactions that occur when two, rather small, gas clouds of partons, clustered in nucleons, bound in the nucleus, collide? Indeed, at first sight, one would be led to believe that the small clouds comprising point-like objects would mutually disperse in the collision, and no localized, dense state of hadronic matter should be formed. It was suggested in some early work, that the two colliding ‘eggs’ should emerge from the high-energy interaction slightly ‘warmed’, but still largely ‘unbroken’. In past few years some of our colleagues have made these eggs not only hot but also scrambled: they believe that somehow this hadronic fireball also develops a high degree of not only (kinetic) thermal, but also chemical equilibration. What does this mean precisely, and can this be true, is what we are going to study in depth here.

Two remarkable properties of hadronic interactions are responsible for deeply inelastic behavior, which could lead to localization of energy in space-time:

- the multiparticle production in hadron-hadron collisions; and
- the effective size of all hadrons expressed in term of their reaction cross sections.

What appears to be a thin system of point-like constituents is effectively already a volume-filling nucleon liquid, which will undergo, in a collision, a rapid self-

multiplication with particle density rising and individual scattering times becoming progressively much shorter than the overall collision time. In historical context, the abundant particle production seen in high energy cosmic ray interactions, has lead Fermi to propose the statistical model of particle production [4]. Our present developments are a natural elaboration of this seminal work, toward a diversified field of many flavored hadron yields, allowing a precision level that a one parameter Fermi-model could of course not reach. Our objective is to account for rapid chemical non-equilibrium dynamics related to formation and sudden disintegration of a new phase of matter.

As the energy available in the collision is increased, the hadron particle/energy density will reach values at which the dissolution of the hadronic constituents into a common deconfined domain will become possible, and indeed must occur according to our knowledge about strong interactions. We do not really know whether deconfinement of hadrons is operating already at AGS energies [5], but there is today no experimental evidence that this low energy range suffices. In contradistinction, a significant number of results obtained at the top SPS energy range can be most naturally interpreted in terms of the formation of a deconfined space–time domain, and this becomes a much more convincing situation once RHIC results are considered. We note that, per participant, there are as many as 7–10 further hadrons produced at SPS energies. This implies that there are thousands of quarks and gluons in the space–time domain of interest, and hence consideration of a ‘local’ (in space–time) equilibrium makes good sense. However, we need to establish which equilibrium is reached, and if not fully, how close are we, and what the deviations from equilibrium tell us about the physics questions we are studying.

In order to establish locally in space and time thermal equilibrium, a rapid equipartition of energy among the different particles present has to occur. Thermal equilibrium can be achieved in principle solely by elastic scattering. Introduction of a (local) temperature  $T$  presupposes that thermal equilibrium has nearly been established. What is the mechanism for the establishment of kinetic momentum distribution equilibrium? The thermalization of the momentum distributions is driven by *all* scattering processes, elastic as well as inelastic, because all of them are associated with exchange of momentum and energy between particles. The *scattering time*, for particles of species  $i$ , is given in terms of the reaction cross section  $\sigma_{ij}$  with particle species  $j$ ,

$$\tau_{i,\text{scatt}} = \frac{1}{\sum_j \langle \sigma_{ij} v_{ij} \rangle \rho_j}. \quad (1)$$

The sum in the denominator is over all available particle species with densities  $\rho_j$ ,  $v_{ij}$  are the relative velocities, and the average is to be taken over the momentum distributions of the particle considered.

It is not hard to ‘guesstimate’ the time scale governing the kinetic equilibration in the QGP. The typical particle–collision time (the inverse of the collision frequency) is obtained from Eq. (1) above. Given the particle densities and soft reaction cross sections, with the relative velocity of these essentially massless components being the velocity of light  $c$ , we find for the quark–gluon plasma scattering time,

$$\tau_i^{\text{QGP}} = 0.2\text{--}2 \text{ fm}, \quad \text{with } \rho_i = 2\text{--}10 \text{ fm}^{-3}, \quad \sigma_i = 2\text{--}5 \text{ mb}, \quad (2)$$

as a range for different particles of type  $i$ , with the shorter time applying to the early high-density stage. This is about an order of magnitude shorter than the time scale for evolution of the fireball, which is derived from the spatial size of the colliding system: for the largest nuclei, in particular the Pb–Pb or Au–Au collisions, over a wide range of energy, we expect

$$\tau^{\text{exp}} \simeq \frac{R_A}{c} \simeq 5\text{--}8 \text{ fm}/c. \quad (3)$$

The achievement of kinetic equilibrium must be visible in the thermal energy spectra, and this behavior, as we argued above, can be understood in qualitative terms using kinetic scattering theory for the case of nuclear collisions. However, it remains to date a mystery why in some important aspects thermal models succeed for the case of  $p$ – $p$  reactions. In particular, the exponential fall off of particle spectra, suggesting thermal equilibrium, has been noted with trepidation for a considerable time.

Hagedorn evaluated this behavior in the experimental data some 35 years ago [1, 2, 3] and he developed the statistical bootstrap model which assumes a statistical phase-space distribution. Hagedorn called it *preestablished or preformed equilibrium*: particles are produced in an elementary interaction with a probability characterized by a universal temperature. We can today only speculate about the physical mechanisms.

In strong interaction physics it is possible that vacuum fluctuations interfere with particle production processes and could generate a preestablished thermal equilibrium distribution. In this case very little additional rescattering is needed for the development of thermal equilibrium. A possible mechanism is that the production of quark pairs by snapping strings is subject to a stochastic vacuum fluctuation force [6], which results in natural Boltzmann distribution of produced quark pairs at just the Hagedorn temperature,  $T_H = 160$  MeV. Another informally discussed possibility is the presence of intrinsic chaotic dynamics capable of rapidly establishing kinetic equilibrium.

Sometimes, the fact that we do not fully understand thermalization in the  $p$ – $p$  case is raised as an argument against the possibility of conventional equilibration in nuclear collisions. We do not think so. In fact, if the  $p$ – $p$  case leads to thermal hadrons, we should have a yet better thermalization in the  $A$ – $A$  case. Thus, a microscopic model that is adopted to extrapolate from  $p$ – $p$  to  $A$ – $A$  collisions should incorporate the concept of the hadronic preestablished thermal equilibrium, else it is not going to be fully successful.

The following stages are today believed to occur in heavy-ion collision:

1. The initial quantum stage.

The formation of a thermalized state within  $\tau_{\text{th}}$  is most difficult to understand, and is subject to intense current theoretical investigation. During the pre-thermal time,  $0 \leq t < \tau_{\text{th}}$ , the properties of the collision system require the study both of quantum transport and of decoherence phenomena, a subject reaching far beyond the scope of this article. In this discussion, we assume that the thermal shape of a (quark, gluon) particle-momentum distribution is reached instantaneously compared with the time scales for chemical equilibration, see section 2. This allows us to sidestep questions regarding the dynamics occurring in the first moments of the heavy-ion interactions, and we explore primarily what happens after a time  $\tau_0 \equiv \tau_{\text{th}} \simeq 0.25$ –

1 fm/c. The value of  $\tau_0$  decreases as the density of the pre-thermal initial state increases, e.g., as the collision energy increases.

2. The subsequent chemical equilibration time.

During the inter-penetration of the projectile and the target lasting no less than  $\sim 1.5$  fm/c, diverse particle-production reactions occur, allowing the approach to chemical equilibrium by light non-strange quarks  $q = u, d$ . As the energy is redistributed among an increasing number of accessed degrees of freedom, the temperature drops rapidly.

3. The strangeness chemical equilibration.

A third time period, lasting up to  $\simeq 5$  fm/c, during which the production and chemical equilibration of strange quarks takes place. There is a reduction of temperature now mainly due to the expansion flow, though the excitation of the strange quark degree of freedom also introduces a non-negligible cooling effect.

4. The hadronization/freeze-out.

The fireball of dense matter expands and decomposes into the final state hadrons, possibly in an (explosive) process that does not allow re-equilibration of the final-state particles. The dynamics is strongly dependent on the size of the initial state and on the nature of the equations of state.

Throughout these stages, a local thermal equilibrium is rapidly established and, as noted, the local temperature evolves in time to accommodate change in the internal structure and size, as is appropriate for an isolated physical system. We have a temperature that passes through the following nearly separable series of stages:

$T_{\text{th}}$	the temperature associated with the initial thermal equilibrium,
$\downarrow$	<i>evolution dominated mainly by production of <math>q</math> and <math>\bar{q}</math>;</i>
$T_{\text{ch}}$	chemical equilibrium of non-strange quarks and gluons,
$\downarrow$	<i>evolution dominated by expansion and production of <math>s</math> and <math>\bar{s}</math>;</i>
$T_{\text{s}}$	condition of chemical equilibrium of $u, d$ and $s$ quark flavors,
$\downarrow$	<i>expansion, dissociation by particle radiation;</i>
$T_{\text{f}}$	temperature at hadron-abundance freeze-out,
$\downarrow$	<i>hadron rescattering, reequilibration; and</i>
$T_{\text{ff}}$	temperature at thermal freeze-out, $T_{\text{ff}} = T(\tau^{\text{exp}})$ .

We encounter a considerable decrease in temperature. The entropy content of an evolving isolated system must increase, and this is initially related to the increase in the number of particles within the fireball and later also due to the increase in volume. However, in the later stages dominated by flow, the practical absence of viscosities in the quark-gluon fluid implies that there is little additional production of entropy. The final entropy content is close to the entropy content established in the earliest thermal stage of the collision at  $t < \tau_0$ , despite a drop in temperature by as much as a factor of two under current experimental RHIC conditions during the sequel evolution of the fireball.

Except for the unlikely scenario of a fireball not expanding, but suddenly disintegrating in the early stage, none of the temperatures discussed above corresponds to the temperature one would read off the (inverse) slopes of particle spectra. In principle, the freeze-out temperature determines the shape of emission and multiplicity of emitted particles. However, the freeze-out occurs within a local flow field of expanding matter and

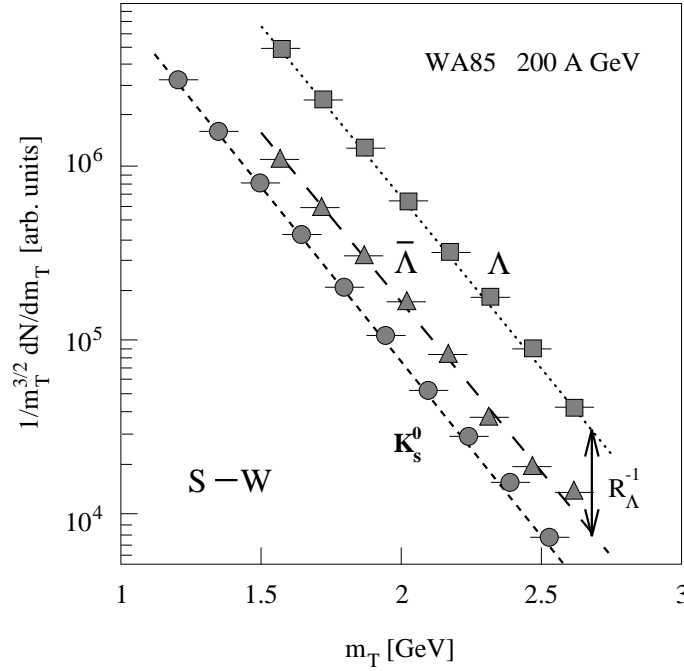


**FIGURE 1.** Strange particle spectra for  $\Lambda$ ,  $\bar{\Lambda}$ , and  $K_S^0$  [7]. The line connecting the  $\Lambda$  and  $\bar{\Lambda}$  spectra, denoted  $R_\Lambda^{-1}$ , shows how at fixed  $m_\perp$  the ratio  $R_\Lambda$  of abundances of these particles can be extracted. Experimental WA85 results at 200A GeV [8, 9, 10].

the thermal spectrum is to be folded with the flow which imposes a Doppler-like shift of  $T_{\text{tf}}$ : we observe a higher temperature than is actually locally present when particles decouple from flowing matter (kinetic or thermal freeze-out). The observable temperature  $T_\perp$  is related to the intrinsic temperature of the source:

$$T_\perp \simeq \frac{1 + \vec{n} \cdot \vec{v}_{\text{tf}}}{\sqrt{1 - \vec{v}_{\text{tf}}^2}} T_{\text{tf}} \rightarrow \sqrt{\frac{1 + v_{\text{tf}}}{1 - v_{\text{tf}}}} T_{\text{tf}}. \quad (4)$$

This relation must be used with caution, since it does not apply in the same fashion to all particles and has a precision rarely better than  $\pm 10\%$ .

To check if thermalization (momentum equilibration) is established, we consider momentum distributions in the direction transverse to the collision axis. Under a Lorentz transformation along the collision axis,  $p_\perp$  remains unchanged and thus

$$m_\perp = \sqrt{m^2 + \vec{p}_\perp^2},$$

is invariant. Transverse mass  $m_\perp$ -particle spectra are not directly distorted by flow motion of the fireball matter along the collision axis, and also no further consideration of the CM frame of reference is necessary, which in fixed target experiments is rapidly moving with respect to a laboratory observer.

In order to study the thermal properties in the fireball as ‘reported’ by the emitted particles, we analyze  $m_\perp$  spectra of many different hadrons. The range of  $m_\perp$ , on the

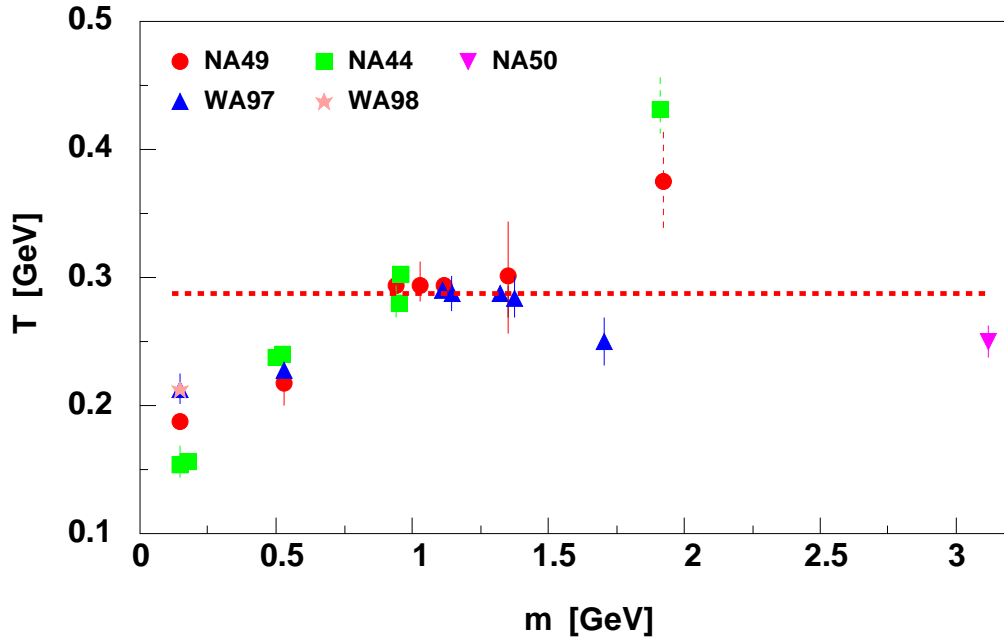


**FIGURE 2.** Inverse slopes  $T_{\perp}$  observed in Pb–Pb interactions at 158A GeV as function of particle mass; symbols indicate the experiment from which data is drawn, as coded in the figure.

one hand, should not reach very large values, at which hadrons originating in hard parton scattering are relevant. On the other hand, we do study relatively small  $m_{\perp}$ , in order to avoid the non-exponential structure associated with transverse matter flow and unstable resonance decays.

The central-rapidity high-transverse-mass spectra of strange particles,  $K_s^0$ ,  $\bar{\Lambda}$ , and  $\Lambda$ , given by the CERN–SPS WA85 collaboration [8, 9, 10],  $m_{\perp}^{-3/2} dN_i/dm_{\perp}$ , are shown in figure 1 on a semi-logarithmic display. The spectra can be fitted with a straight line. Similar results were also reported from the related work of the WA94 collaboration for S–S interactions [11]. We see, in figure 1, in the region of transverse masses presented,  $1.5 \text{ GeV} < m_{\perp} < 2.6 \text{ GeV}$ , that the behaviors of all three different particles feature the same inverse exponential slope,  $T_{\perp} = 232 \pm 5 \text{ MeV}$ . This is not the actual temperature of the fireball, as noted in Eq. (4).

Presence of matter flow which generates the relatively high value of spectral slope is also responsible for differences in the observed values of  $T_{\perp}$  for particles of widely different mass such as pions, kaons and nucleons considered in a similar  $p_{\perp}$  interval. This is illustrated in figure 2. A remarkable feature is that many strange baryons are seen to have similar inverse slope, as is also seen in table 1.

## 2. CHEMICAL EQUILIBRIA

The average energy of each particle defines the local temperature  $T$ , good for all particles. A local chemical potentials  $\sigma_i$  need to be introduced for each kind of particle ‘ $i$ ’ in

**TABLE 1.** Inverse slopes  $T_{\perp}$  for various strange hadrons.

	$\Lambda$	$\bar{\Lambda}$	$\Xi^-$	$\Xi^+$	$\Omega^- + \bar{\Omega}^+$	$\phi$
Pb–Pb	$289 \pm 2$	$287 \pm 4$	$286 \pm 9$	$284 \pm 17$	$251 \pm 19$	$305 \pm 15$
S–W	$233 \pm 3$	$232 \pm 7$	$244 \pm 12$	$238 \pm 16$		

order to establish the particle density. We will see that it is often more convenient to use particle fugacity,

$$\Upsilon_i \equiv e^{\sigma_i/T}. \quad (5)$$

The statistical parameters  $T$  and  $\sigma_i$  (or  $\Upsilon_i$ ) express different types of equilibration processes in the hadron matter fireball, and in general there is a considerable difference in the time needed for the attainment of thermal and, respectively, chemical equilibrium.

The fugacity controls, independently of temperature, the yield of the particle species. For Boltzmann statistics, the fugacity  $\Upsilon_i$  is multiplying the particle distribution, which in local rest frame assumes the usual form,

$$\frac{d^6 N_i}{d^3 p d^3 x} = g_i \frac{\Upsilon_i}{(2\pi)^3} e^{-E_i/T}. \quad (6)$$

For the Fermi/Bose quantum distributions the fugacity factor remains in front of the exponential,

$$\frac{d^6 N_i^{\text{F/B}}}{d^3 p d^3 x} = \frac{g_i}{(2\pi)^3} \frac{1}{\Upsilon_i^{-1} e^{E_i/T} \pm 1}, \quad (7)$$

The coefficient  $g_i$  is the degeneracy of the particle considered, it comprises the intrinsic properties such as spin and color of the particle.

The number of particles ‘ $i$ ’ present is the result of momentum integral of the phase-space distribution. Thus the yield of particles depends on both temperature and the fugacity. However, fugacity practically does not control the shape of the momentum distribution, and thus it is generally said that it can be chosen to produce the required particle density, with temperature being the parameters determining the momentum distribution.

The allowed range of the (always positive) fugacities is not restrained for Boltzmann and Fermi particles. However for bosons, the condensation singularity of the distribution cannot be crossed, which requires that

$$\Upsilon_i \leq e^{m_i/T}. \quad (8)$$

As usual the  $E_i(p) > m_i$  for all  $p$  and  $m_i$  is the particle rest mass. Almost never the exceptional value  $\Upsilon_i = 1$  applies, with the exception of an chemically equilibrated gas of particles (such as photons) which do not carry any charge, i.e., a conserved, discrete quantum number.

As the number of particles evolves in a reaction, the fugacities usually change. For example, we begin with small initial yield of strange quarks and antiquarks in a deconfined

quark-gluon plasma. Subsequent reactions of the type,



increase the yield of pairs of strange quarks and if we could cook the hadronic matter at a constant temperature  $T$  (thermal bath), than after some time known as the chemical relaxation time, the yield of strange quarks and antiquarks would approach the chemical equilibrium yields corresponding to the fugacity approaching unity,

$$\Upsilon_{i=s}(t) = \Upsilon_{i=\bar{s}}(t) \rightarrow 1. \quad (10)$$

The important message here is that the particle fugacities are time dependent and can evolve rapidly during the heavy-ion collision process. Description of the dynamical evolution of the fugacity is one of the challenges we are facing in order to understand the physics of hadronization.

Another important challenge which is arising, is due to the presence of two quite different types of chemical equilibria.

- In relativistic reactions, particles can be made as energy is converted to matter. Therefore, we can expect to approach slowly the *absolute* chemical equilibrium. Absolute chemical equilibrium is hard to grasp intuitively, since our instincts are distorted by the fact that a black body photon radiator is correctly assumed to be in absolute chemical equilibrium on the time scale defined by a blink of an eye. We characterize the approach to absolute chemical equilibrium by a fugacity factor  $\gamma_i$  for particle ‘ $i$ ’. We will evaluate the evolution of  $\gamma_i$  in the heavy-ion collision reaction as a function of time. Given its physical meaning it is often referred to as the phase-space occupancy.
- *Relative* chemical equilibration, the case commonly known in chemistry. It involves reactions that distribute or maintain a certain already existent element among different accessible compounds. Use of chemical potentials associated with conserved global properties, such as  $\mu_b$  for baryon number, presupposes that the particular relative chemical equilibrium is present. For example production of quarks in pairs assures that there is always the same net flavor (thus baryon number) balance, and hence the relative flavor equilibrium is maintained. The chemical potential of antiparticles is in consequence the negative of that for particles, *provided* that we have introduced appropriate  $\gamma_i$  to control the absolute yield of particle-antiparticle pairs.

In general the fugacity of each individual particle will comprise the two chemical factors associated with the two different chemical equilibria. For example, let us look at the nucleon, and the antinucleon:

$$\Upsilon_N = \gamma_N e^{\mu_b/T}, \quad \Upsilon_{\bar{N}} = \gamma_N e^{-\mu_b/T}. \quad (11)$$

Equivalently, we can keep separate chemical potentials for particles and antiparticles [12, 13],

$$\sigma_N \equiv \mu_b + T \ln \gamma_N, \quad \sigma_{\bar{N}} \equiv -\mu_b + T \ln \gamma_N. \quad (12)$$

There is an obvious difference between the two chemical factors in Eq.(11): the number of nucleon-antinucleon pairs is associated with the value of  $\gamma_N$  but not with  $\mu_b$ .



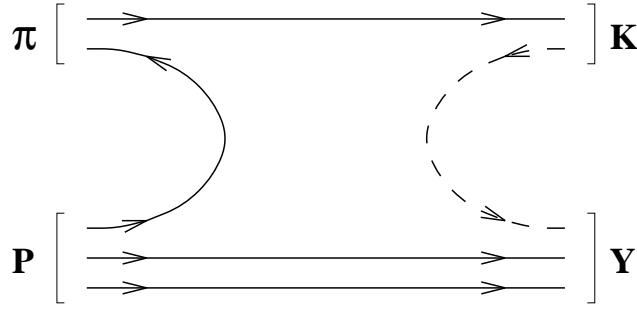


**FIGURE 3.** The production of strangeness in reactions of the type  $\pi + N \rightarrow K + Y$  in the HG phase. Solid lines indicate the flow of light quarks and the disappearance of one  $\bar{q}q$  pair, the dashed line is for the added  $\bar{s}s$  pair.

This can be seen looking at the first law of thermodynamics, in this context written as:

$$\begin{aligned} dE &= -P dV + T dS + \sigma_N dN + \sigma_{\bar{N}} d\bar{N} \\ &= -P dV + T dS + \mu_b (dN - d\bar{N}) + T \ln \gamma_N (dN + d\bar{N}). \end{aligned} \quad (13)$$

To obtain the second form we have employed Eq. (12). We see that  $\mu_b$  is the energy required to change the baryon number,

$$b \equiv N - \bar{N},$$

by one unit, while the number of nucleon-antinucleon pairs,

$$2N_{\text{pair}} \equiv N + \bar{N},$$

is related to  $\gamma_N$ . For  $\gamma_N = 1$  the last term vanishes, at this point small fluctuation in number of nucleon pairs does not influence the energy of the system, we are have reached the absolute baryochemical equilibrium.

Presence of  $\gamma_N$  allows us to count and control within a theoretical description how many pairs of nucleons are added. When  $\gamma_N \rightarrow 1$ , we have as many as we would expect in absolute chemical equilibrium, of course establishing chemical equilibrium for anti-nucleons can take a long time. However, it is not uncommon to see in contemporary literature assumption of instantaneous absolute chemical equilibrium,  $\gamma_i \rightarrow 1$ , with particles ‘instantaneously’ reaching their absolute chemical equilibrium abundances. The argument presented is that such a simple model ‘works’, as it is capable to describe widely different particle yields qualitatively. This in fact is the observation which motivated Hagedorn’s work. 40 years after, our foremost interest is to understand the deviations from this, in order to unravel the mechanism by which such a surprising result can arise.

In order to better understand the difference between absolute and relative chemical equilibrium, let us consider the abundance of strangeness in the baryon-rich hadronic gas (HG) phase. There is little ‘strangeness’ initially, strangeness is made in collision processes of the interacting hadronic matter. We begin far from absolute chemical-strangeness equilibrium. To make  $s\bar{s}$  pairs in a HG phase, there are many possible reactions, classified usually as the direct- and associate-production processes. In the

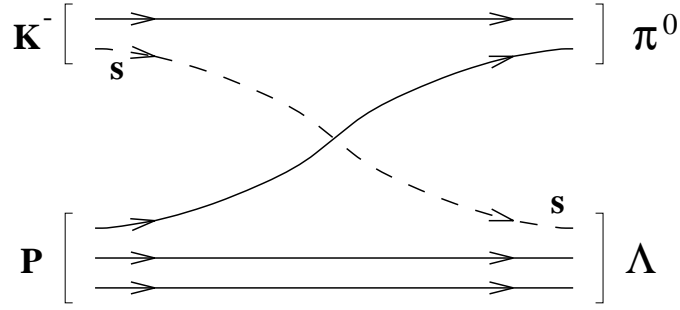


**FIGURE 4.** An example of a strangeness-exchange reaction in the HG phase:  $K^- + p \rightarrow \Lambda + \pi^0$ . Solid lines, flow of  $u$  and  $d$  quarks; dashed line, exchange of an  $s$  quark between two hadrons.

associate production process, a pair of strange quarks is shared between two existent hadrons, of which one is a baryon, typically a nucleon  $N$ , which becomes a hyperon  $Y$ :



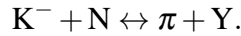
This situation is illustrated in figure 3.

In a direct-production process, a pair of strangeness-carrying particles is formed directly via annihilation of two mesons, adding a pair to the system:



Here, a pair of strange particles is made in the form of a pair of kaons,  $K^+K^-$ .

With these two reaction types alone it could be that populations of strange mesons and baryons evolve differently. However, the meson carrier of the  $s$  quark,  $K^-$ , can exchange this quark, see figure 4, via fast exothermic reaction with a nucleon, forming a hyperon:



This reaction establishes relative chemical equilibrium between mesons and baryons by being able to move the strange quark between these two different strangeness carriers,  $s\bar{q}$  mesons and  $sq\bar{q}$  baryons.

Reactions establishing the redistribution of existent flavor, or the abundance of some other conserved quantity, play a different role from the reactions that actually contribute to the formation of this flavor, or other quantum number, and facilitate the approach to absolute chemical equilibrium. Accordingly, the time constants for relaxation are different, since different types of reaction are involved.

Apart from the different relaxation times associated with the different types of thermal and chemical equilibria, there are different time scales associated with the different fundamental interactions involved. For example, the electro-magnetic interactions are considerably slower at reaching equilibrium than are the strong interactions governing the evolution of dense hadronic fireballs created in ultra-relativistic heavy-ion collisions. All the important time constants for relaxation in heavy-ion collisions arise from differences in mechanisms operating within the realm of strong interactions. Therefore, the separation of time scales is not as sharp as that between the different interactions, though a clear hierarchy arises and we have presented it above.

There are just a few chemical potentials which suffice in the study of hadronic matter. It is convenient to use the quark flavor for this purpose, since there is a continuity in the notation across the phase boundary of quark matter and hadronic matter. We thus use:

$$\lambda_u = e^{\mu_u/T}, \quad \lambda_d = e^{\mu_d/T}, \quad \lambda_s = e^{\mu_s/T}. \quad (14)$$

Since more often than not the light flavors  $u, d$  remain indistinguishable one often uses:

$$\mu_q = \frac{1}{2}(\mu_u + \mu_d), \quad \lambda_q^2 = \lambda_u \lambda_d. \quad (15)$$

Considering that three quarks make a baryon we also have

$$\mu_b = 3\mu_q, \quad \lambda_b = \lambda_q^3. \quad (16)$$

It is important to remember that the three quark flavors  $u, d, s$  carry baryon number. Thus when baryon density is evaluated this has to be appropriately allowed for, counting all three quark densities. This can be easily forgotten for strangeness, considering the usual definition of baryochemical potential, Eq. (16).

At this point, we recall the relationship of strange quark chemical potential and strangeness chemical  $\mu_S$  potential (as opposed to strange quark chemical potential  $\mu_s$ ):

$$\mu_s = \frac{1}{3}\mu_b - \mu_S, \quad \lambda_s = \frac{\lambda_q}{\lambda_S}, \quad (17)$$

which expresses the fact that strange quarks carry negative strangeness and one third of baryon number. Consequently, hyperons have negative strangeness, antihyperons positive strangeness,  $K^-(\bar{u}s)$  negative strangeness and thus it is called antikaon  $\bar{K}$ , and  $K^+(u\bar{s})$  has positive strangeness, and it is the kaon  $K$ . This nomenclature has an obvious historical origin, when strangeness was first discovered, the  $\bar{s}$  containing  $K^+$  has been the particle produced.

Using Eq. (17) in statistical formulation allows to evaluate baryon number and strangeness by simply differentiating the grand canonical partition function  $\mathcal{Z}$ :

$$N_b = \lambda_b \frac{\partial \mathcal{Z}(\beta, \lambda_b, \lambda_S)}{\partial \lambda_b}, \quad N_S = \lambda_S \frac{\partial \mathcal{Z}(\beta, \lambda_b, \lambda_S)}{\partial \lambda_S}, \quad (18)$$

where as usual  $\beta = 1/T$ . Especially the computation of  $N_b$  is more cumbersome when  $\lambda_i, i = u, d, s$ , is used.

On the other hand, we believe that the use of fugacities which follow the yield of quarks,  $\lambda_i, i = u, d, s$ , is intuitive and easy in programing, mistakes are rather difficult to make. Particle yields can be easily followed and checked, and thus errors and omissions minimized. As an example, let us consider the ratio of a baryon and antibaryon with strangeness and for reasons which will become obvious in a moment we choose to look at the ratio  $\bar{\Xi}^-(\bar{d}\bar{s}\bar{s})/\Xi^-(dss)$ . Given the quark content and ignoring isospin asymmetry we find:

$$\frac{\bar{\Xi}^-}{\Xi^-} = \frac{\lambda_s^{-2}\lambda_q^{-1}}{\lambda_s^2\lambda_q} = \lambda_s^{-4}\lambda_q^{-2} = \frac{e^{2\mu_s/T}e^{-\mu_b/T}}{e^{-2\mu_s/T}e^{\mu_b/T}} = e^{4\mu_s/T}e^{-2\mu_b/T}. \quad (19)$$

Since all  $\Xi$  resonances which contribute to this ratio are symmetric for particles and antiparticles, and possible weak interaction feed from  $\overline{\Omega}(\overline{s}\overline{s}\overline{s})$  and, respectively  $\Omega(sss)$  are small, these expressions are actually rather exactly giving the expected experimental ratio.

When we check the results presented by [14], we find for the freeze-out parameters stated there  $T = 174$  MeV,  $\mu_b = 46$  MeV and  $\mu_s = 13.6$  MeV, a ratio  $\overline{\Xi^-}/\Xi^- = 0.806$ , which differs from the result  $\overline{\Xi^-}/\Xi^- = 0.894$  given. While the difference appears small, when looked at in terms of the particle chemical potential this is a big effect: Considering that the Cascades have baryon number  $b = 1$  and strangeness  $S = -2$ , we expect that the  $\Xi$ -chemical potential is  $\mu_{\Xi}|_{\text{expected}} = \mu_b - 2\mu_s = 18.8$  MeV. On the other hand given the result seen in [14],

$$0.894 = \frac{\overline{\Xi^-}}{\Xi^-} = e^{-2\mu_{\Xi}/T}.$$

The particle chemical potential is  $\mu_{\Xi}|_{\text{used}} = 9.75$  MeV. In order to approach using the stated potentials the answer presented in [14], we can try to use another quark fugacity definition,

$$\left. \frac{\overline{\Xi^-}}{\Xi^-} \right|_{\text{PBM}} \equiv \frac{\lambda_s^2 \lambda_q^{-1}}{\lambda_s^{-2} \lambda_q} = e^{\frac{2}{3}\mu_b/T - 4\mu_s/T} = 0.87. \quad (20)$$

However, this redefinition is not consistent with the ratios of particles such as  $K^-/K^+$  also seen in [14]. This example of a possible partial misunderstanding of the quantum numbers associated with different hadrons illustrates the danger of using anything but the (valance) quark fugacities in study of chemical properties of hadrons.

To complete the discussion of chemical potentials, we need to address the  $u$ - $d$  asymmetry which is only noticeable for Pb-Pb interactions at SPS. We complement Eq. (15) by introducing

$$\mu_I = \mu_d - \mu_u, \quad \lambda_I = \frac{\lambda_d}{\lambda_u} \geq 1. \quad (21)$$

In the last inequality, we show the constraint arising given that nuclei have in general a greater neutron than proton number. The subscript  $I$  reminds us of isospin, we have also used  $\delta\mu$  for  $\mu_I$  in the past. A sensitive probe of  $\lambda_I$  is the ratio

$$\frac{\pi^-(\overline{u}d)}{\pi^+(u\overline{d})} = \lambda_I^2. \quad (22)$$

At RHIC, for  $\sqrt{s_{NN}} = 130$  GeV, the outflow of projectile and target matter from the central rapidity region leaves a very small 'input' isospin asymmetry: with a baryon density per unit rapidity at  $dN_b/dy \simeq 20$ , but hundreds of mesons made, the valance quark asymmetry is negligible. However, at the top energy at SPS there is an effect at the level of 2–4% percent, since baryon number is retained in the fireball and the meson to baryon ratio is 8 times smaller, as measured in terms of the ratio of all negative hadrons,

$$h^- = \pi^- + K^- + \overline{p}, \quad (23)$$

to baryon number. At SPS, we have  $h^-/b \simeq 2$ , while at RHIC at  $\sqrt{s_{NN}} = 130$  GeV,  $h^-/b \simeq 16.5$ , in both cases at central rapidity. We can estimate for SPS where  $\lambda_q = 1.6$ :

$$1.6 < \lambda_d < 1.66, \quad 1.54 < \lambda_u < 1.6.$$

The exact value of  $\lambda_d, \lambda_u$  depends on what form of matter (confined, deconfined) is the source of particles produced, and the influence of gluon fragmentation into quark pairs. The limiting values are found ignoring gluon fragmentation and evaluating the ratio of all down and up quarks in hot quark matter, where quark density is  $\rho_i \propto \mu_i T^2, i = u, d$ . Thus we find

$$\frac{\rho_d}{\rho_u} = 1 + \delta = \frac{\mu_d}{\mu_u}, \quad \delta = \frac{n-p}{n+2p}, \quad (24)$$

where  $n(udd)$  and  $p(uud)$  are the neutron, and respectively, proton input into the quark matter source. For heavy nuclei  $\delta \simeq 0.156$ , and we find:

$$\lambda_d = \lambda_q^{\frac{1}{1-\delta/2}}, \quad \lambda_u = \lambda_q^{\frac{1}{1+\delta/2}}. \quad (25)$$

We now return to discuss further the characterization of chemical non-equilibrium. When we study the approach to chemical equilibrium for different hadrons, we can use three non-equilibrium parameters,  $\gamma_u, \gamma_d, \gamma_s$ , and equivalently,  $\gamma_q^2 = \gamma_u \gamma_d$ . In quark matter, these three factors express the approach to the expected chemical equilibrium yield by the quark abundances. Upon hadronization quarks are redistributed among all individual hadrons and the non-equilibrium abundances can be characterized by the same three factors only, since in all hadron formation reactions only quark-antiquark pairs of the same flavor can be formed. It is important to realize that even if there were no change of the quark pair number in hadronization, the values of  $\gamma_u, \gamma_d, \gamma_s$  in hadron gas and quark matter must differ since the phase spaces have different size as we shall discuss further below. In general, we have to distinguish  $\gamma_u^{\text{QGP}}, \gamma_d^{\text{QGP}}, \gamma_s^{\text{QGP}}$  from  $\gamma_u^{\text{HG}}, \gamma_d^{\text{HG}}, \gamma_s^{\text{HG}}$ . Moreover, as noted these sets of parameters differ due to hadronization of gluons into quark pairs.

We thus characterize the fugacities of all hadrons by six parameters. For baryons the typical examples are (considering protons  $p(uud)$ , antiprotons  $\bar{p}(\bar{u}\bar{u}\bar{d})$ ,  $\Lambda(uds)$ ,  $\bar{\Omega}(\bar{s}\bar{s}\bar{s})$  as examples):

$$\Upsilon_p = \gamma_u^2 \gamma_d e^{2\mu_u + \mu_d}, \quad \Upsilon_{\bar{p}} = \gamma_u^2 \gamma_d e^{-2\mu_u - \mu_d}, \quad \Upsilon_{\Lambda} = \gamma_u \gamma_d \gamma_s e^{\mu_u + \mu_d + \mu_s}, \quad \Upsilon_{\bar{\Omega}} = \gamma_s^3 e^{-3\mu_s}. \quad (26)$$

The yield of mesons follows the same pattern (considering  $\pi^+(u\bar{d})$ ,  $\pi^-(\bar{u}d)$ ,  $K^-(\bar{u}s)$ ,  $\phi(\bar{s}s)$  as examples):

$$\Upsilon_{\pi^+} = \gamma_u \gamma_d e^{\mu_u - \mu_d}, \quad \Upsilon_{\pi^-} = \gamma_u \gamma_d e^{-\mu_u + \mu_d}, \quad \Upsilon_{K^-} = \gamma_u \gamma_s e^{-\mu_u + \mu_s}, \quad \Upsilon_{\phi} = \gamma_s^2. \quad (27)$$

It is important to note that this approach assumes that the relative population of heavier resonances is in chemical equilibrium with the lighter states, since we have the same value of  $\Upsilon$  for all hadrons with the same valance quark content. For example  $\Upsilon_p = \Upsilon_{\Delta^+}$ . We thus realize that this approach solely focuses on the quark distribution and does not allow for the possibility that heavier resonances may simply not be populated. This

method thus is most suitable for a hadronizing quark matter fireball, and may miss important features of a hadron fireball which never entered the deconfined phase. When conditions are present which let us believe that the population of important heavier resonance states such as  $\Delta(qqq)$  could be suppressed beyond the thermal factor  $\propto e^{m_\Delta/T}$  we have to restore a factor  $\gamma_\Delta < \gamma_q^3$  which allows for such suppression. As long as this is not done, we in fact assume that the relative abundances of hadronic states of same quark content are in chemical equilibrium. The following study of deviations from chemical equilibrium is addressing a much more subtle question, namely how the overall number of (valence) quarks compares to the hadron phase-space chemical equilibrium expectations.

### 3. HOW NEAR TO CHEMICAL EQUILIBRIUM?

Is such a characterization of hadron abundances at all functioning, and is so, how close are we actually to absolute chemical equilibrium in heavy-ion reactions? To answer this question a systematic test was performed for the S–W/Pb 200A GeV experimental SPS results [15]. Particle yields were fitted allowing progressively greater and greater degree of chemical non-equilibrium. The results in table 2 show that the statistical significance is increasing with progressively greater chemical ‘freedom’. Since the statistical significance which can be reached is satisfactory, it appears that the quark counting suffices to describe the yields of heavier hadron resonances.

We note, in the last row in table 2, that while the yield of strangeness is still suppressed as compared to expectations based on absolute chemical equilibrium, the number of light quarks seen exceeds the count expected. Another way to say the same thing is that there is pion excess, or alternatively, entropy excess [16, 17, 18]. In fact there is a maximum value that  $\gamma_q$  can assume: consider again Eq. (7) for pions, assuming symmetry for  $u, d$  quarks:

$$f_\pi \equiv \frac{d^6 N_i^\pi}{d^3 p d^3 x} = \frac{3}{(2\pi)^3} \frac{1}{\gamma_q^{-2} e^{E_\pi/T} - 1}. \quad (28)$$

We see that for

$$\gamma_q \rightarrow e^{m_\pi/2T} = \gamma_q^c, \quad (29)$$

the Bose condensation becomes possible.

**TABLE 2.** Statistical parameters obtained from fits of data for S–Au/W/Pb collisions at 200A GeV, without enforcing conservation of strangeness [15].

$\lambda_q$	$\lambda_s$	$\gamma_s$	$\gamma_q$	$\chi^2/\text{dof}$
$1.52 \pm 0.02$	1*	1*	1*	17
$1.52 \pm 0.02$	$0.97 \pm 0.02$	1*	1*	18
$1.48 \pm 0.02$	$1.01 \pm 0.02$	$0.62 \pm 0.02$	1*	2.4
$1.49 \pm 0.02$	$1.00 \pm 0.02$	$0.73 \pm 0.02$	$1.22 \pm 0.06$	0.90

\* denotes fixed (input) values

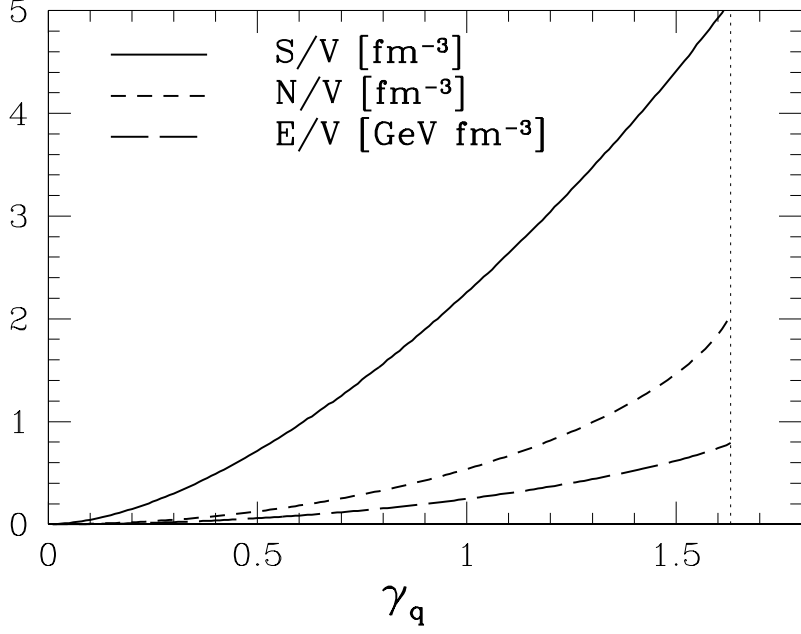


**FIGURE 5.** Pion-gas properties  $N/V$  for particles,  $E/V$  for energy, and  $S/V$  for entropy density, as functions of  $\gamma_q$  at  $T = 142$  MeV.

The properties of the pion gas as function of  $\gamma_q$  are shown in figure 5, where the entropy, energy and particle number is expressed in terms of the momentum distribution function by:

$$\frac{S}{V} = \int d^3 p [(1 + f_\pi) \ln(1 + f_\pi) - f_\pi \ln f_\pi], \quad (30)$$

$$\frac{E}{V} = \int d^3 p \sqrt{m_\pi^2 + p^2} f_\pi, \quad (31)$$

$$\frac{N}{V} = \int d^3 p f_\pi. \quad (32)$$

There is significant rise in entropy content as  $\gamma_q$  grows toward the singular value. Excess entropy of a possibly color deconfined source can thus be squeezed in hadronization into a hadron phase comprising an over saturated pion gas. Indeed, when we perform an analysis of particles produced in the Pb–Pb 158A GeV reactions, as well as at RHIC, the value  $\gamma_q^c$  is always favored by a fit having a statistical significance [19].

When an analysis of the Pb–Pb collision system is performed allowing for quark pair abundance chemical non-equilibrium, we find that the light quark phase-space occupancy parameter  $\gamma_s$  prefers the maximum allowed  $\gamma_q^c$ , and this is also the numerical value preferred by the strange quark occupancy parameter  $\gamma_s$ . The freeze-out of particles is found at  $T = 150$  MeV. The velocity of (transverse) expansion  $v_c$  (not further discussed here) is at half velocity of light. These results were obtained fitting all particles shown in table 3.

**TABLE 3.** WA97 (top) and NA49 (bottom) Pb–Pb 158A GeV-collision hadron ratios compared with phase-space fits.

Ratios	Reference	Experimental data	Pb  $s; \gamma_q$	Pb  $\gamma_q$
$\Xi/\Lambda$	[20]	$0.099 \pm 0.008$	0.096	0.095
$\bar{\Xi}/\bar{\Lambda}$	[20]	$0.203 \pm 0.024$	0.197	0.199
$\bar{\Lambda}/\Lambda$	[20]	$0.124 \pm 0.013$	0.123	0.122
$\bar{\Xi}/\Xi$	[20]	$0.255 \pm 0.025$	0.251	0.255
$K^+/K^-$	[21]	$1.800 \pm 0.100$	1.746	1.771
$K^-/\pi^-$	[22]	$0.082 \pm 0.012$	0.082	0.080
$K_s^0/b$	[23]	$0.183 \pm 0.027$	0.192	0.195
$h^-/b$	[24]	$1.970 \pm 0.100$	1.786	1.818
$\phi/K^-$	[25]	$0.145 \pm 0.024$	0.164	0.163
$\bar{\Lambda}/\bar{p}$	$y = 0$		0.565	0.568
	$\chi^2$		1.6	1.15
	$N; p; r$		9; 4; 1	9; 5; 1

Due to their exceptional inverse slope, see figure 2, the yields of both  $\Omega$  and  $\bar{\Omega}$  are known, to follow different systematic behavior and have not been considered in this fit. With the parameters here determined the yields of  $\bar{\Omega}$  are under predicted. This excess yield originates at the lowest  $m_\perp$ , as we shall discuss below, see figure 10. The ‘failure’ of a statistical-hadronization model to describe yields of soft  $\Omega$  and  $\bar{\Omega}$  has several possible explanations. One is the possibility that an enhancement in production of  $\Omega$  and  $\bar{\Omega}$  is caused by pre-clustering of strangeness in the deconfined phase [26]. This would enhance the production of all multistrange hadrons, but most prominently the highly phase-space-suppressed yields of  $\Omega$  and  $\bar{\Omega}$ . This mechanism would work only if pairing of strange quarks near to the phase transition were significant. Another possible mechanism of  $\Omega$  and  $\bar{\Omega}$  enhancement is the distillation of strangeness [27, 28], followed by breakup of strangelets (strangeness enriched quark drops) which could contribute to production of  $\Omega$  and  $\bar{\Omega}$ . The decay of disoriented chiral condensates has recently been proposed as another source of soft  $\Omega$  and  $\bar{\Omega}$  [29].

In view of these pre- and post-dictions of the anomalous yield of  $\Omega$  and  $\bar{\Omega}$ , and the difference in shape of particle spectra, we believe that one should abstain from introducing these particles into statistical-hadronization-model fits. We note that the early statistical descriptions of yields of  $\Omega$  and  $\bar{\Omega}$  have not been sensitive to the problems we described [30, 31]. In fact, as long as the parameter  $\gamma_q$  is not considered, it is not possible to describe the experimental data at the level of precision that would allow recognition of the excess yield of  $\Omega$  and  $\bar{\Omega}$  within statistical hadronization model. For example, a chemical-equilibrium fit, which includes the yield of  $\Omega$  and  $\bar{\Omega}$ , has for 18 fitted data points with two parameters a  $\chi^2/\text{dof} = 37.8/16$  [32]. Such a fit is quite unlikely to contain all the physics, even if its appearance to the naked eye suggests that a very good description of experimental data as been achieved.

We also see, in table 4, the yield of strangeness obtained in the fit of the final state hadron phase-space, which with 0.7 strange pairs per baryon appears large. The question we next consider is what we should have expected in hadronization of a deconfined quark



**TABLE 4.** Upper section: the statistical model parameters which best describe the experimental results for Pb–Pb data seen in table 3. Bottom section: energy per entropy, anti-strangeness, and net strangeness of the full hadron phase-space characterized by these statistical parameters. In column two, we fix  $\lambda_s$  by the requirement of conservation of strangeness.

	Pb  $_{\nu}^{s,\gamma_q}$	Pb  $_{\nu}^{\gamma_q}$
$T$ [MeV]	$151 \pm 3$	$147.7 \pm 5.6$
$v_c$	$0.55 \pm 0.05$	$0.52 \pm 0.29$
$\lambda_q$	$1.617 \pm 0.028$	$1.624 \pm 0.029$
$\lambda_s$	1.10*	$1.094 \pm 0.02$
$\gamma_q$	$\gamma_q^{c*} = e^{m_{\pi}/(2T_f)} = 1.6$	$\gamma_q^{c*} = e^{m_{\pi}/(2T_f)} = 1.6$
$\gamma_s/\gamma_q$	$1.00 \pm 0.06$	$1.00 \pm 0.06$
$E/b$ [GeV]	4.0	4.1
$s/b$	$0.70 \pm 0.05$	$0.71 \pm 0.05$
$E/S$ [MeV]	$163 \pm 1$	$160 \pm 1$
$(\bar{s} - s)/b$	0*	$0.04 \pm 0.05$

\* indicates values resulting from constraints.

matter phase. We consider the ratio of the equilibrium density of strangeness, arising in the Boltzmann-gas limit, to the baryon density in a fireball of quark–gluon plasma:

$$\frac{\rho_s}{\rho_b} = \frac{s}{b} = \frac{s}{q/3} = \frac{\gamma_s^{\text{QGP}} (3/\pi^2) T^3 W(m_s/T)}{\gamma_q^{\text{QGP}} \frac{2}{3} (\mu_q T^2 + \mu_q^3/\pi^2)}. \quad (33)$$

$W(x) = x^2 K_2(x)$  defines in Boltzmann limit the equilibrium strange-quark density, with  $g_s = 6$ . We assume that to a first approximation, perturbative thermal QCD corrections, cancel out in the ratio. For  $m_s = 200$  MeV and  $T = 150$  MeV, we have

$$\frac{s}{b} \simeq \frac{\gamma_s^{\text{QGP}}}{\gamma_q^{\text{QGP}}} \frac{0.7}{\ln \lambda_q + (\ln \lambda_q)^3/\pi^2}. \quad (34)$$

The relative yield  $s/b$  is mainly dependent on the value of  $\lambda_q$ . In the approximation considered, it is nearly temperature-independent, the result is shown in figure 6, as a function of  $\lambda_q - 1$  (the variable chosen to enlarge the interesting region  $\lambda_q \rightarrow 1$ ) for  $\gamma_s^{\text{QGP}} = \gamma_q^{\text{QGP}} = 1$ . At the top SPS energy where  $\lambda_q \rightarrow 1.5$ – $1.6$ , we see that the equilibrium yield is at 1.5 pairs of strange quarks per participating baryon. Considering the experimental yield in table 4, we thus conclude  $\gamma_s^{\text{QGP}} \sim 0.5$ . Experimentally the directly accessible observable is the occupancy of the hadron-strangeness phase-space and we show in table 4,  $\gamma_s^{\text{HG}} \simeq 1.6$ . This thus implies that in the hadronization of a presumed QGP the smaller phase-space of hadrons is overpopulated by a QGP abundance, even when it is originally in the QGP phase well below the equilibrium value.

The above analysis demonstrated the importance of the study of quark-pair abundance chemical non-equilibrium features and how these are capable to refine our understanding of the QGP formation and hadronization.

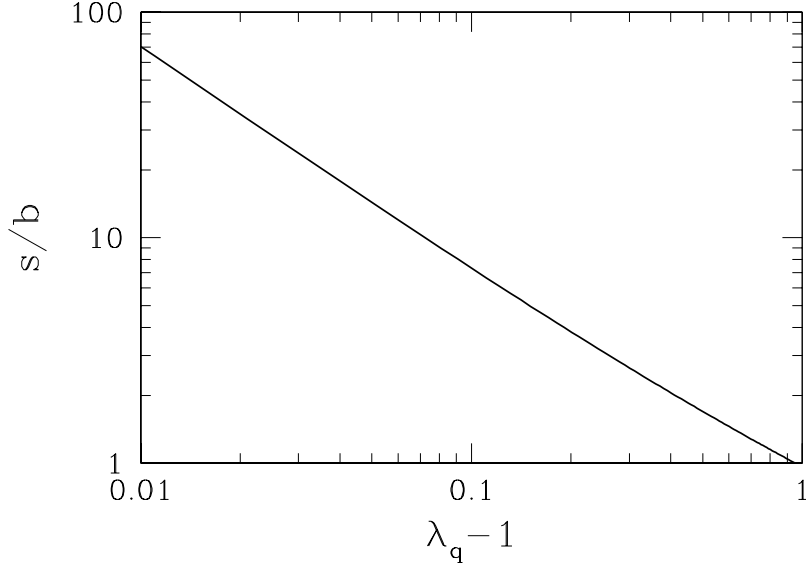


**FIGURE 6.** The yield of strangeness per baryon as a function of  $\lambda_q$  in equilibrated quark–gluon plasma.

#### 4. QGP AND CHEMICAL ANALYSIS

An interesting feature seen in table 2 is that the value of  $\lambda_s$  converges to unity. This is not at all what could be expected for a equilibrated hadron gas. Namely, the value of  $\lambda_s$  arises from the requirement of conservation of strangeness. Specifically the net strangeness is given by,

$$0 = \langle n_s \rangle - \langle n_{\bar{s}} \rangle = \frac{T^3}{2\pi^2} \left[ (\lambda_s \lambda_q^{-1} - \lambda_s^{-1} \lambda_q) \gamma_s \gamma_q F_K + (\lambda_s \lambda_q^2 - \lambda_s^{-1} \lambda_q^{-2}) \gamma_s \gamma_q^2 F_Y \right. \\ \left. + 2(\lambda_s^2 \lambda_q - \lambda_s^{-2} \lambda_q^{-1}) \gamma_s^2 \gamma_q F_{\Xi} + 3(\lambda_s^3 - \lambda_s^{-3}) \gamma_s^3 F_{\Omega} \right], \quad (35)$$

where we have employed the phase-space integrals for known hadrons,

$$F_K = \sum_j g_{K_j} W(m_{K_j}/T); \quad K_j = K, K^*, K_2^*, \dots, \quad m \leq 1780 \text{ MeV}, \\ F_Y = \sum_j g_{Y_j} W(m_{Y_j}/T); \quad Y_j = \Lambda, \Sigma, \Sigma(1385), \dots, \quad m \leq 1940 \text{ MeV}, \\ F_{\Xi} = \sum_j g_{\Xi_j} W(m_{\Xi_j}/T); \quad \Xi_j = \Xi, \Xi(1530), \dots, \quad m \leq 1950 \text{ MeV}, \\ F_{\Omega} = \sum_j g_{\Omega_j} W(m_{\Omega_j}/T); \quad \Omega_j = \Omega, \Omega(2250). \quad (36)$$

The  $g_i$  are the spin–isospin degeneracy factors,  $W(x) = x^2 K_2(x)$ , where  $K_2$  is the modified Bessel function.

In general, Eq. (35) must be equal to zero since strangeness is a conserved quantum number with respect to the strong interactions, and no strangeness is brought into

the reaction. The possible exception is dynamic evolution with asymmetric emission of strange and antistrange hadrons [28]. Eq. (35) can be solved analytically when the contribution of multistrange particles is small:

$$\lambda_s|_0 = \lambda_q \sqrt{\frac{F_K + \gamma_q \lambda_q^{-3} F_Y}{F_K + \gamma_q \lambda_q^3 F_Y}}. \quad (37)$$

We thus see that except for a very exceptional point where the kaon and hyperon strangeness phase-spaces for a given value of baryochemical properties are of same magnitude, the value of  $\lambda_s$  will not be unity. One can of course force the hadron multiplicity description to this value, but the prize one pays is a greatly reduced statistical significance [32, 33], where chemical equilibrium has been assumed. We note that for the value  $\lambda_s = 1$ , we can analytically solve Eq. (35), including the effect of multistrange hadrons and obtain:

$$\mu_b = 3T \ln(x + \sqrt{x^2 - 1}), \quad 1 \leq x = \frac{F_K - 2\gamma_s F_\Xi}{2\gamma_q F_Y}. \quad (38)$$

In what situation is the value  $\lambda_s \rightarrow 1$  natural? This value will arise when for all baryochemical conditions the strange and antistrange quark numbers can balance independently. This will in most cases be in the phase in which strange quarks can roam freely. In this case we have instead of condition Eq. (35),

$$\begin{aligned} 0 &= \langle n_s \rangle - \langle n_{\bar{s}} \rangle \\ &= g \int \frac{d^3 p}{(2\pi)^3} \left( \frac{1}{1 + \gamma_s^{-1} \lambda_s^{-1} \exp\left(\frac{\sqrt{p^2 + m_s^2}}{T}\right)} - \frac{1}{1 + \gamma_s^{-1} \lambda_s \exp\left(\frac{\sqrt{p^2 + m_s^2}}{T}\right)} \right). \end{aligned} \quad (39)$$

We note the change in the power of  $\lambda_s$  between these two terms, and recognize that this integral can vanish only for  $\lambda_s \rightarrow 1$ .

There is potentially small but significant asymmetry in  $\lambda_s$  due to the Coulomb charge present in baryon-rich quark matter: long-range electromagnetic potential  $V_C \neq 0$  influence strange and antistrange particles differently, and a slight deviation  $\lambda_s > 1$  is needed in order to compensate for this effect in the QGP phase. We have as generalization of Eq. (39) [34],

$$\begin{aligned} 0 &= \langle N_s \rangle - \langle N_{\bar{s}} \rangle \\ &= g \int_{R_f} \frac{d^3 r d^3 p}{V(2\pi)^3} \left( \frac{1}{1 + \gamma_s^{-1} \lambda_s^{-1} e^{(E(p) - \frac{1}{3} V_C(r))/T}} - \frac{1}{1 + \gamma_s^{-1} \lambda_s e^{(E(p) + \frac{1}{3} V_C(r))/T}} \right), \end{aligned} \quad (40)$$

which clearly cannot vanish for  $V_C \neq 0$ , in the limit  $\lambda_s \rightarrow 1$ . The volume integral is here over the fireball of size  $R_f$ . In the Boltzmann approximation one easily finds that

$$\tilde{\lambda}_s \equiv \lambda_s \ell_C^{1/3} = 1, \quad \ell_C \equiv \frac{\int_{R_f} d^3 r e^{V/T}}{\int_{R_f} d^3 r}. \quad (41)$$

$\ell_C < 1$  expresses the Coulomb deformation of strange quark phase-space.  $\ell_C$  is not a fugacity that can be adjusted to satisfy a chemical condition, since consideration of  $\lambda_i$ ,  $i = u, d, s$ , exhausts all available chemical balance conditions for the abundances of hadronic particles, and allows introduction of the fugacity associated with the Coulomb charge of quarks and hadrons. Instead,  $\ell_C$  characterizes the distortion of the phase-space by the long-range Coulomb interaction. This Coulomb distortion of the quark phase-space is naturally also present for  $u, d$  quarks, but appears less significant given that  $\lambda_u$  and  $\lambda_q$  are empirically determined. On the other hand, this effect eliminates much if not all the difference between  $\mu_u$  and  $\mu_d$  we have described above, since the quark abundance asymmetry arises naturally due to Coulomb effect — said differently, the Coulomb effect deforms the phase-space such that it is natural to have more  $d$  than  $u$  quarks and thus the asymmetry between  $\lambda_d$  and  $\lambda_u$  is reduced.

Choosing  $T = 140$  MeV and  $m_s = 200$  MeV, and noting that the value of  $\gamma_s$  is practically irrelevant since this factor cancels out in the Boltzmann approximation we find for  $Z_f = 150$  that the value  $\lambda_s = 1.10$  is needed for  $R_f = 7.9$  fm, whereas for S–Au/W/Pb reactions, similar analysis leads to a value  $\lambda_s = 1.01$ . Chemical freeze-out at higher temperature, e.g.,  $T = 170$  MeV, leads for  $\lambda_s = 1.10$  to somewhat smaller radii, which is consistent with the higher temperature used.

The fit of the Pb–Pb system seen in table 4 converged just to the value expected if QGP were formed. However, accidentally for  $\gamma_q = \gamma_q^c$  this happens also to be where in hadronic gas strangeness balance is found. Thus in case of Pb–Pb the indication from chemistry that a QGP has been formed arises mainly from the fact that a significant entropy excess is available, (light quark-pair excess) and the strange quark-pair excess, seen the relatively high value of  $\gamma_s \simeq \gamma_q$  in table 4. When compared to the yield expected from QGP, this implies that  $\gamma_s^{\text{HG}}/\gamma_s^{\text{QGP}} \simeq 3$ . To better understand this, we compare the phase-space of strangeness in quark–gluon plasma with that of the resulting hadronic gas. The absolute strangeness yields must be the same in both phases. We perform the comparison assuming that in a fast hadronization of QGP neither temperature  $T$ , nor the baryochemical potential  $\mu_b$ , nor the reaction volume have time to change, the difference in the properties of the phases is absorbed in the change in the occupancy of phase-space,  $\gamma_i$  in the two phases.

We relate the two phase-space occupancies in HG and QGP, by equating the strangeness content in the two phases. One has to keep in mind that there is some additional production of strangeness due to gluon hadronization, however, this is not altering the argument presented significantly. On canceling out the common normalization factor  $T^3/(2\pi^2)$ , we obtain

$$\gamma_s^{\text{QGP}} V^{\text{QGP}} g_s W \left( \frac{m_s}{T^{\text{QGP}}} \right) \simeq \gamma_s^{\text{HG}} V^{\text{HG}} \left( \frac{\gamma_q \lambda_q}{\lambda_s} F_K + \frac{\gamma_q^2}{\lambda_q^2 \lambda_s} F_Y \right). \quad (42)$$

Here we have, without loss of generality, followed the  $\bar{s}$ -carrying hadrons in the hadronic gas phase-space, and we have omitted the contribution of multistrange antibaryons for simplicity. We now use the condition that strangeness is conserved, Eq. (37), to eliminate  $\lambda_s$  from Eq. (42), and obtain (making explicit which statistical

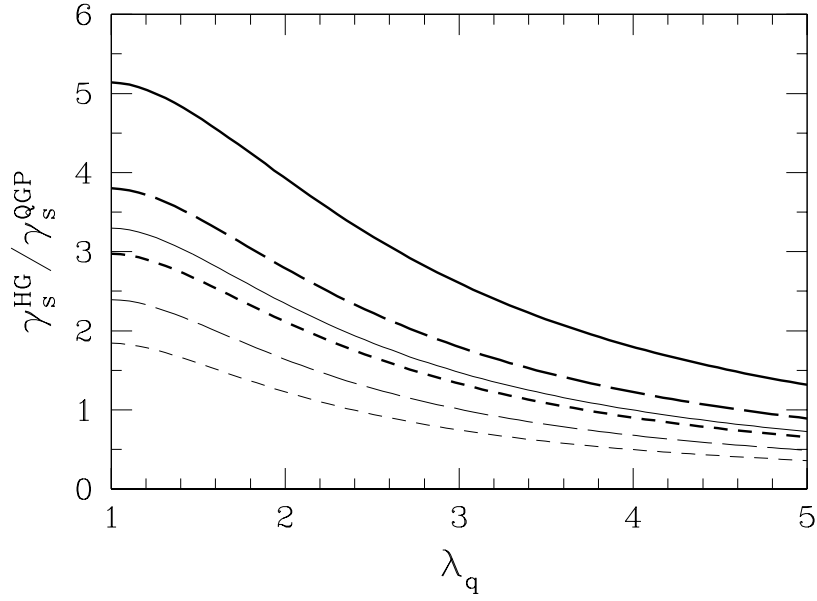


**FIGURE 7.** The HG/QGP strangeness-occupancy  $\gamma_s$  ratio in sudden hadronization as a function of  $\lambda_q$ . Solid lines,  $\gamma_q^{\text{HG}} = 1$ ; long-dashed lines,  $\gamma_q^{\text{HG}} = 1.3$ ; and short-dashed lines,  $\gamma_q^{\text{HG}} = 1.6$ . Thin lines are for  $T = 170$  and thick lines for  $T = 150$  MeV, for both phases.

parameter occurs in which phase)

$$\frac{\gamma_s^{\text{HG}}}{\gamma_s^{\text{QGP}}} \frac{V^{\text{HG}}}{V^{\text{QGP}}} = \frac{g_s W(m_s/T^{\text{QGP}})}{\sqrt{(\gamma_q F_K + \gamma_q^2 \lambda_q^{-3} F_Y)(\gamma_q F_K + \gamma_q^2 \lambda_q^3 F_Y)}}. \quad (43)$$

This ratio is shown in figure 7, and the two lines of particular interest are the thin solid line (chemical equilibrium  $\gamma_q^{\text{HG}} = 1$  with  $T = 170$  MeV in hadronic gas phase), and the short dashed thick line ( $\gamma_q^{\text{HG}} = 1.6$  at  $T = 150$  MeV) which correspond to the two hadronization scenarios which can be used to fit the SPS experimental results. We see that, near to the established value  $\lambda_q \simeq 1.6$ , both yield a squeeze by factor 3 for the ratio of the strangeness phase-space occupancies.

This result implies that hadronization of QGP is at SPS and RHIC accompanied by an increase by factor three in the value of  $\gamma_s$  and thus it is most important to allow in the study of particle yields for this off-equilibrium property, otherwise the tacit assumption has been made that QGP has not been formed. If at RHIC conditions are reached in which strangeness in QGP is closer to absolute chemical equilibrium,  $\gamma_s^{\text{QGP}} \rightarrow 1$ , even a more significant overpopulation by strangeness of the hadronic gas phase would result,  $\gamma_s^{\text{HG}} \rightarrow 3$ .

## 5. THERMAL FREEZE-OUT AND SINGLE FREEZE-OUT

The non-equilibrium features introduced into the chemical analysis reduce the chemical freeze-out temperature to values close to those expected for the thermal freeze-out, that is when the spectral shape of particles freezes out after at a low particle density also elastic hadron interactions cannot occur. One is thus tempted to ask the question if both freeze-out conditions (chemical and thermal) are not actually one and the same. The confirmation came when we found that the spectra and yields of hyperons, antihyperons and kaons were very well described within this scenario. However, we could not publish the results of a single freeze-out scenario at SPS [35], our scientific findings disagreed with personal opinion of than associate editor of The Physical Review Letters, Herr Ulrich Heinz. Our submission to PRL (dated March 8, 1999) occurred on the same day as the submission to Physics Letters B of the two-freeze-out chemical equilibrium, however this work was published [32], which as history has often shown makes a lot of difference.

Despite this setback we proceeded to enlarge on our single-freeze-out sudden hadronization picture for SPS, which in our opinion was strongly supported by many experimental facts, and we could present these results at meetings [36]. Specifically, the spectra of strange hadrons and anti-hadrons show universal slope, see figure 2, which supports such a single freeze-out scenario decisively. The understanding of pion spectra is very difficult since many (yet undiscovered) resonances contribute in a relevant fashion, and the soft part of the spectrum is particularly prone to ‘deformation’ by hadronization mechanisms and unknown matter flows [37]. Thus we report here on our precise study of spectra of kaons and hyperons [38].

The final particle distribution is composed of directly produced particles and decay products of heavier hadronic resonances:

$$\frac{dN_X}{dm_\perp} = \left. \frac{dN_X}{dm_\perp} \right|_{\text{direct}} + \sum_{\forall R \rightarrow X+2+\dots} \left. \frac{dN_X}{dm_\perp} \right|_{R \rightarrow X+2+\dots}. \quad (44)$$

$R(M, M_T, Y) \rightarrow X(m, m_T, y) + 2(m_2) + \dots$ , where we indicate by the arguments that only for the decay particle  $X$  we keep the information about the shape of the momentum spectrum.

In detail, the decay contribution to yield of  $X$  is:

$$\frac{dN_X}{dm_\perp^2 dy} = \frac{g_r b}{4\pi p^*} \int_{Y_-}^{Y_+} dY \int_{M_{T_-}}^{M_{T_+}} dM_T^2 \frac{M}{\sqrt{p_T^2 p_T'^2 - \{ME^* - M_T m_T \cosh \Delta Y\}^2}} \frac{d^2 N_R}{dM_T^2 dY}, \quad (45)$$

We have used  $\Delta Y = Y - y$ , and  $\sqrt{s}$  is the combined invariant mass of the decay products other than particle  $X$  and  $E^* = (M^2 - m^2 - m_2^2)/2M$ ,  $p^* = \sqrt{E^{*2} - m^2}$  are the energy, and momentum, of the decay particle  $X$  in the rest frame of its parent. The limits on the integration are the maximum values accessible to the decay product  $X$ :

$$Y_\pm = y \pm \sinh^{-1} \left( \frac{p^*}{m_T} \right), \quad M_{T_\pm} = M \frac{E^* m_T \cosh \Delta Y \pm p_T \sqrt{p^{*2} - m_T^2} \sinh^2 \Delta Y}{m_T^2 \sinh^2 \Delta Y + m^2}.$$

The theoretical primary particle spectra (both those directly produced and parents of decay products) are derived from the Boltzmann distribution by Lorenz-transforming from a flowing intrinsic fluid element to the CM-frame, and integrating over allowed angles between particle direction and local flow.

We introduce in the current analysis two velocities: a local flow velocity  $v$  of the fireball matter where from particles emerge, and hadronization surface (breakup) velocity which we refer to as  $v_f^{-1} \equiv dt_f/dx_f$ . Particle production is controlled by the effective volume element, which comprises this quantity. In detail:

$$dS_\mu p^\mu = d\omega \left( 1 - \frac{\vec{v}_f^{-1} \cdot \vec{p}}{E} \right), \quad d\omega \equiv \frac{d^3x d^3p}{(2\pi)^3}. \quad (46)$$

The Boltzmann distribution we adapt has thus the form

$$\frac{d^2N}{dm_T dy} \propto \left( 1 - \frac{\vec{v}_f^{-1} \cdot \vec{p}}{E} \right) \gamma m_T \cosh y e^{-\gamma \frac{E}{T} \left( 1 - \frac{\vec{v} \cdot \vec{p}}{E} \right)}, \quad (47)$$

where  $\gamma = 1/\sqrt{1-v^2}$ . The normalization for each hadron type  $h = X, R$  is  $N^h = V_{\text{QGP}} \prod_{i \in h} \lambda_i \gamma_i$ . We use the chemical parameters  $\lambda_i$  and  $\gamma_i$ ,  $i = q, s$ , as obtained in the chemical analysis.

The experimental data we consider are published  $m_\perp$  distribution [39], with additional information obtained about absolute normalization. This allowed us to perform the spectral shape analysis together with yield analysis, which indicates that the reaction volume is increasing as expected with the centrality of the reaction. This said, we will only focus here on the question if the shape of the spectra is consistent with the chemical freeze-out condition [38]. The best fit to the spectra in fact produces the temperature and transverse velocity in excellent agreement with those inferred from chemical analysis we have discussed above.

We show, in figure 8, the parameters determining the shape of the  $m_\perp$  distributions, that is  $T, v, v_f$ , as function of the centrality for scattering bin 1, 2, 3, 4 with the most central bin being 4. The horizontal lines delineate range of result of the chemical analysis.

There is no indication of a significant, or systematic, change of  $T$  with centrality. This is consistent with the believe that the physics we are considering arises in all centrality bins explored by the experiment WA97 in Pb–Pb reactions at 158A GeV, i.e., for the number of participants greater than 60. Only most peripheral interactions produce a change in the pattern of strange hadron production [40, 41], and we are anticipating with deep interest the more peripheral hyperon spectra which should become available from experiment NA57. The magnitudes of the collective expansion velocity  $v$  and the break-up (hadronization) speed parameter  $v_f$  also do not show dependence on centrality, though within the experimental error, one could argue inspecting figure 8 (right) that there is systematic increase in transverse flow velocity  $v$  with centrality and thus size of the system. Such an increase is expected, since the more central events comprise greater volume of matter, which allows more time for development of the flow. Interestingly, it is in  $v$ , and not in  $T$ , that the slight change of spectral slopes noted in the presentation of the experimental data [39] is found.

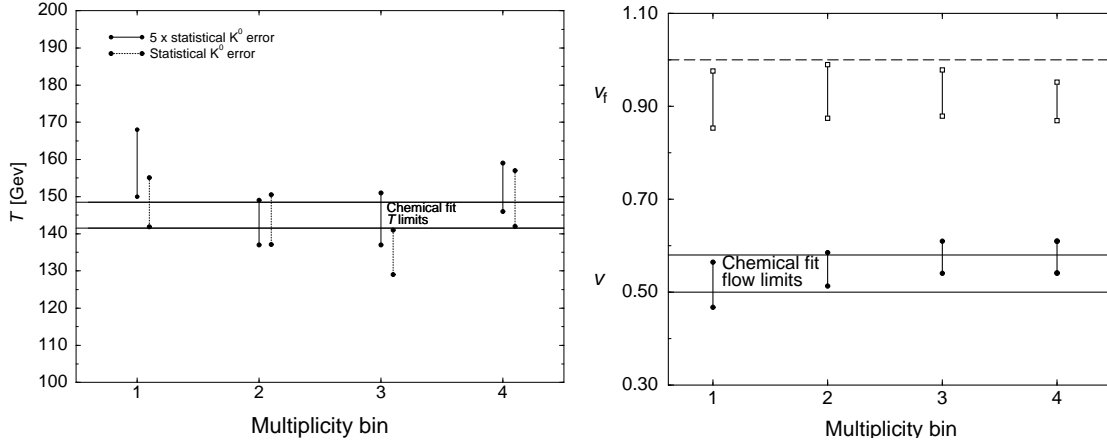


**FIGURE 8.** The thermal freeze-out temperature  $T$  (left), flow velocity  $v$  (bottom right), and breakup (hadronization hyper-surface-propagation) velocity  $v_f$  (top right) for various collision-centrality bins. The upper limit  $v_f = 1$  (dashed line) and chemical-freeze-out-analysis limits for  $v$  (solid lines) are also shown. For the temperature, results obtained with increased error for kaon spectra are also shown.

The value of the beak-up (hadronization) speed parameter  $v_f$  shown in the top portion (right) of figure 8 is near to velocity of light which is consistent with the picture of a sudden breakup of the fireball. This hadronization surface velocity  $v_f$  was in the chemical fit fixed to be equal to  $v$ , as there was not enough sensitivity in purely chemical fit to determine the value of  $v_f$ .

It is important to explicitly check how well the particle  $m_{\perp}$ -spectra are reproduced. We group all centrality bin spectra and show, in figure 9,  $\Lambda$ ,  $\bar{\Lambda}$ ,  $\Xi$  and  $\bar{\Xi}$ . Overall, the description of the shape of the hyperon spectra is very satisfactory. In figure 10 on left we see for the four centrality bins the spectra for the sum  $\Omega + \bar{\Omega}$ . The two lowest  $m_{\perp}$  data points are systematically under predicted. Some deviation at high  $m_{\perp}$  may be attributable to acceptance uncertainties, also seen in the the  $\Xi$  results. This low  $m_{\perp}$  enhancement of  $\Omega + \bar{\Omega}$  is at the origin of the low value of the inverse slope and the associated excess of  $\Omega, \bar{\Omega}$  compared to the chemical freeze-out analysis. Unlike with chemical analysis where the  $\Omega, \bar{\Omega}$  have been omitted, the relatively large statistical errors allowed us to include the  $\Omega$ -spectra in the fit procedure, which is dominated by the other hyperons and kaons. This allows to see how the deviation from the systematics established by other hyperons and kaons is arising. In fact the low  $m_{\perp}$ -bins of the  $\Omega + \bar{\Omega}$  experimental spectrum with experimental yield excess at 1–2 s.d. translate into 3 s.d. deviations from the yields generated in the chemical analysis.

For kaons  $K^0$  (figure 10 on right) the statistical errors are very small, and we find in a more in depth statistical analysis that they must be smaller than the systematic errors not considered. For this reason we have presented earlier in figure 8 results for temperatures obtained with both statistical, and 5 times greater than statistical error for kaons. This increased value was used in the fit with objective to asses the influence of the unknown systematic error. The stability of the result implies that statistically precise kaons do not overwhelm the fit procedure of hyperons, and/or that the hyperon and kaon results are consistent with the model employed.



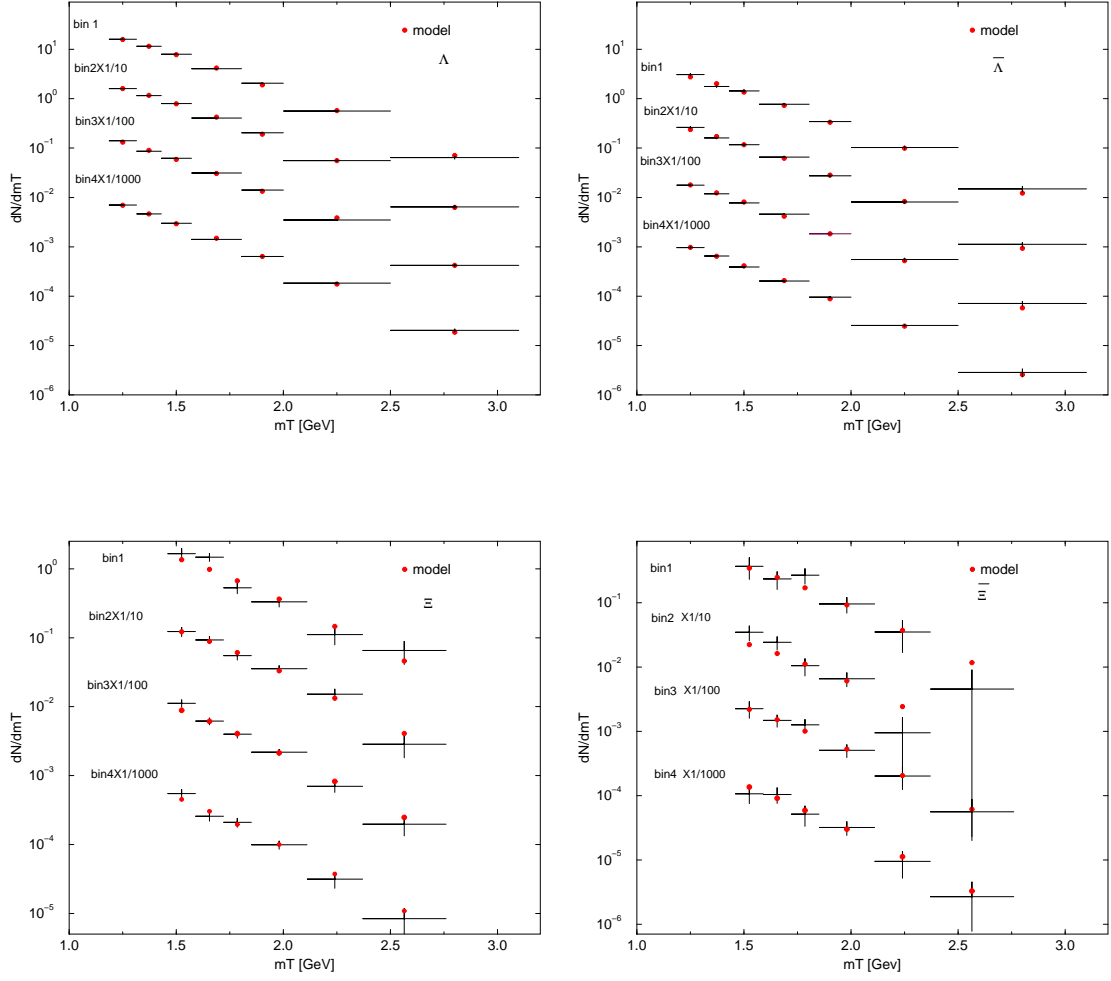


**FIGURE 9.** Thermal analysis  $m_T$  spectra:  $\Lambda$  (top left),  $\bar{\Lambda}$  (top right)  $\Xi$  (bottom left),  $\bar{\Xi}$  (bottom right).

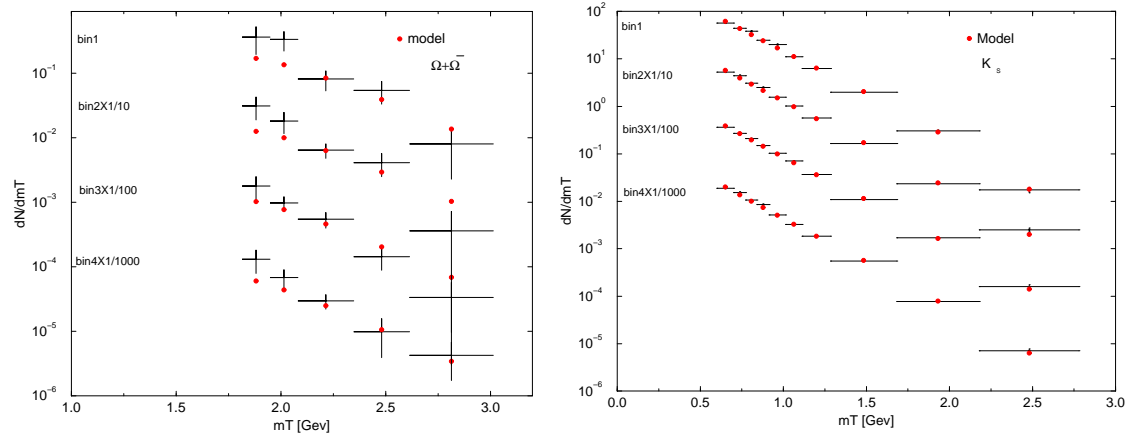


**FIGURE 10.** Thermal analysis  $m_T$  spectra:  $\Omega + \bar{\Omega}$  (left) and  $K_s$  (right).

Overall, we see that the description of kaon and hyperon spectra with the parameters obtained in chemical freeze-out analysis if possible, indeed we conclude from the above study that the thermal analysis is proving the conclusion that both thermal and chemical freeze-out occur at the same condition of temperature and transverse velocity, as one would expect in sudden break up of a deconfined supercooled quark–gluon plasma. Strange hadrons at SPS originate in single freeze-out reaction.

## 6. RHIC-130 HADRON ABUNDANCE ANALYSIS, ROUND IIB

The strangeness yield observed in 158–200A GeV reactions corresponds to  $\mathcal{O}(0.7)$ - $s\bar{s}$ -pairs of quarks per participant baryon. We estimate that this is corresponding to 50% QGP phase-space occupancy, thus considerably more extreme results on strangeness can arise at RHIC and with it greater anomalies in strange baryon and antibaryon enhancement. The experimental STAR and PHENIX collaboration results considered here were obtained at  $\sqrt{s_{\text{NN}}} = 130$  GeV in the central-rapidity region, for the most central (5–7%) collision reactions. The particle production results available as of QM2002 meeting (Nantes, July 2002) allow a rather good understanding of the physical conditions established at the chemical hadron freeze-out at RHIC, and we use the opportunity to update our analysis.

Due to the approximate longitudinal scaling for the central rapidity results the effects of longitudinal flow at central rapidity cancels out and we can evaluate the full phase-space yields in order to obtain particle ratios. In our following analysis, we do not include natural results such as  $\pi^+/\pi^- = 1$ , which can be expected since the large hadron yield combined with the flow of baryon isospin asymmetry toward the fragmentation rapidity region assures this result to within a great precision, as we have discussed in section 2. We also do not fit the results for  $K^*$  and  $\bar{K}^*$  since the reconstructed yields depend on the degree of rescattering of resonance decay products [42]. We consider here 19 particle ratios seen in table 5. We favor consideration of particle ratios, since this allows us to combine ratios from different experiments with slightly different trigger conditions, and reduces systematic errors. We have used published experimental ratios and also formed ratios of rapidity densities reported by one and the same experiment.

We present in table 5 in three last columns the results for both chemical equilibrium (last column) and non-equilibrium fits, *i.e.* in the latter case we fix the chemical parameters to their equilibrium value. We observe a considerable improvement in the statistical significance of the results of chemical non-equilibrium fits (see bottom line), as we have seen in our related earlier RHIC work [43, 44], in consistency with the situation at SPS. Next to the fitted results, we show in parenthesis the contribution to the error ( $\chi^2$ ) for each entry. We consider only statistical errors for the experimental results, since much of the systematic error should cancel in the particle ratios. However, we do not allow, when pion multiplicity is considered, that errors are smaller than  $\simeq 8\%$ , which is our estimated error in the theoretical evaluation of the pion yield due to incomplete understanding of the high mass hadron resonances. Some of the experimental results are thus shown with a theoretical error. When such an enlargement of the experimental error is introduced, a dagger as superscript appears in second column in table 5 below.

**TABLE 5.** Fits of central-rapidity hadron ratios at  $\sqrt{s_{NN}} = 130$  GeV. Top section: experimental results, followed in middle by chemical parameters (results of fits), and the physical properties of the phase-space obtained from evaluation of final state hadron phase-space, and the fitting error. Columns: ratio considered, data value with reference, the non-equilibrium fit with 100%  $\Xi \rightarrow Y$  cascading ( $f_{\Xi} = 1$ ) and 40%  $Y \rightarrow N$  ( $f_{\Lambda} = 0.4$ ), the non-equilibrium fit with 40%  $\Xi \rightarrow Y$  and 40%  $Y \rightarrow N$ , and in the last column, the chemical equilibrium fit with 40% cascading. The superscript \* indicates quantities fixed by constraints and related considerations. The superscript † indicates the error is dominated by theoretical considerations. Subscripts  $\Xi, \Lambda$  mean that these values include weak cascading. In parenthesis we show the contribution of the particular result to the total  $\chi^2$ .

	Data	Ref.	100% $\Xi \rightarrow Y$ 40% $Y \rightarrow N$	40% $\Xi \rightarrow Y$ 40% $Y \rightarrow N$	40% $\Xi \rightarrow Y$ 40% $Y \rightarrow N$
$\bar{p}/p$	$0.71 \pm 0.06$	[45]	0.672(0.4)	0.678(0.3)	0.689(0.1)
$\bar{\Lambda}_{\Xi}/\Lambda_{\Xi}$	$0.71 \pm 0.04$	[46]	0.759(1.0)	0.748(0.9)	0.757(1.4)
$\bar{\Xi}/\Xi$	$0.83 \pm 0.08$	[47]	0.794(0.2)	0.804(0.1)	0.816(0.0)
$K^-/K^+$	$0.87 \pm 0.07$	[48]	0.925(0.6)	0.924(0.6)	0.934(0.8)
$K^-/\pi^{\pm}$	$0.15 \pm 0.02^{\dagger}$	[48]	0.159(0.2)	0.161(0.3)	0.150(0.0)
$K^+/\pi^{\pm}$	$0.17 \pm 0.02^{\dagger}$	[48]	0.172(0.0)	0.174(0.1)	0.161(0.2)
$\bar{\Lambda}_{\Xi}/h^-$	$0.059 \pm 0.004^{\dagger}$	[46]	0.057(0.3)	0.050(5.1)	0.045(11.9)
$\bar{\Lambda}_{\Xi}/h^-$	$0.042 \pm 0.004^{\dagger}$	[46]	0.043(0.0)	0.037(1.3)	0.034(3.8)
$\bar{\Lambda}_{\Xi}/p$	$0.90 \pm 0.12$	[45]	0.832(0.3)	0.691(3.0)	0.491(11.6)
$\bar{\Lambda}_{\Xi}/\bar{p}$	$0.93 \pm 0.19$	[45]	0.929(0.0)	0.763(0.8)	0.539(4.2)
$\pi^{\pm}/p_{\Lambda}$	$9.5 \pm 2$	[48]	9.4(0.0)	9.2(0.5)	7.6(22.8)
$\pi^{\pm}/\bar{p}_{\Lambda}$	$13.4 \pm 2.5$	[48]	13.7(0.1)	13.4(0.0)	10.9(7.9)
$\Xi^-/\pi$	$0.0088 \pm 0.0008^{\dagger}$	[47, 49]	0.0096(1.0)	0.0103(3.6)	0.0067(7.1)
$\Xi^-/h^-$	$0.0085 \pm 0.0015$	[47, 49]	0.0079(0.1)	0.0084(0.0)	0.0054(4.3)
$\bar{\Xi}^-/h^-$	$0.0070 \pm 0.001$	[47, 49]	0.0063(0.5)	0.0068(0.1)	0.0044(6.7)
$\Xi^-/\Lambda$	$0.193 \pm 0.009$	[49]	0.195(0.1)	0.196(0.1)	0.132(45.2)
$\bar{\Xi}^-/\Lambda$	$0.221 \pm 0.011$	[49]	0.213(0.6)	0.214(0.4)	0.144(48.7)
$\bar{\Omega}/\bar{\Xi}^-$			0.205	0.21	0.18
$\bar{\Omega}/\bar{\Xi}^-$			0.22	0.23	0.20
$\bar{\Omega}/\Omega$	$0.95 \pm 0.1$	[49]	0.87(0.7)	0.88(0.5)	0.89(0.4)
$\bar{p}/h^-$			0.046	0.049	0.063
$\phi/K^-$	$0.15 \pm 0.03$	[49]	0.178(0.9)	0.185(1.3)	0.146(0.0)
$T$			$140.1 \pm 1.1$	$142.3 \pm 1.2$	$164.3 \pm 2.2$
$\gamma_q^{\text{HG}}$			1.64*	1.63*	1*
$\lambda_q$			$1.070 \pm 0.008$	$1.0685 \pm 0.008$	$1.065 \pm 0.008$
$\mu_b$ [MeV]			28.4	28.3	31.0
$\gamma_s^{\text{HG}}/\gamma_q^{\text{HG}}$			$1.54 \pm 0.04$	$1.54 \pm 0.04$	1*
$\lambda_s$			1.0136*	1.0216*	1.0196*
$\mu_S$ [MeV]			6.1	6.4	7.1
$E/b$ [GeV]			35.0	34.6	34.8
$s/b$			9.75	9.7	7.2
$S/b$			234.8	230.5	245.7
$E/S$ [MeV]			148.9	150.9	141.5
$\chi^2/\text{dof}$			7.1/(19-3)	19/(19-3)	177.2/(19-2)

As is today well understood, the high yields of hyperons require significant corrections for unresolved weak decays. Some experimental results are already corrected in

this fashion: the weak cascading corrections were applied to the most recent  $p$  and  $\bar{p}$  results by the PHENIX collaboration [45], and in the  $\Xi/\Lambda$  and  $\bar{\Xi}/\bar{\Lambda}$  ratio of the STAR collaboration we use here [47, 49]. However, some of the results we consider are not yet corrected [48, 46], and are indicated in the first column in table 5 by a subscript  $\Lambda$  or  $\Xi$ .

The subscript  $\Lambda$  means that the cascading of hyperons into nucleons has to be included while fitting the particle ratio considered, and we have found that a 35-40% cascading ( $f_\Lambda = 0.35-0.4$ ) is as expected favored by the fits of pion to nucleon ratio. Similarly, the subscript  $\Xi$  indicates that the  $\Xi$  cascading into single strange hyperons  $Y = \Sigma, \Lambda$  was also not corrected for in the considered result. Here we find empirically that full acceptance of the Cascades into singly strange hyperons is favored, again by both equilibrium and non-equilibrium fits ( $f_\Xi \rightarrow 1$ ). We also include in the  $\Xi$  and  $\Lambda$  yield with the appropriate branching the weak decay of  $\Omega$ , with the experimental acceptance fraction being the same as in the decay of  $\Xi$  ( $f_\Omega = f_\Xi$ ).

In other words, in the results shown in table 5, the hyperon yields are:

$$\begin{aligned}\Lambda_\Xi &= \Lambda_{\text{th}} + \Sigma_{\text{th}}^0 + f_\Xi(2\Xi_{\text{th}}^- + \Omega_{\text{th}}), & \bar{\Lambda}_\Xi &= \bar{\Lambda}_{\text{th}} + \bar{\Sigma}_{\text{th}}^0 + f_\Xi(2\bar{\Xi}_{\text{th}}^- + \bar{\Omega}_{\text{th}}^-); \\ p_\Lambda &= p_{\text{th}} + f_\Lambda 0.77\Lambda_\Xi, & \bar{p}_\Lambda &= \bar{p}_{\text{th}} + f_\Lambda 0.77\bar{\Lambda}_\Xi; \\ \Xi^- &= \Xi_{\text{th}}^- + 0.08\Omega_{\text{th}}^-, & \bar{\Xi}^- &= \bar{\Xi}_{\text{th}}^- + 0.086\bar{\Omega}_{\text{th}}^-.\end{aligned}$$

Here subscript ‘th’ indicates statistical model yields. The factor ‘2’ preceding  $\Xi_{\text{th}}^-$ ,  $\bar{\Xi}_{\text{th}}^-$  allows for the decay of  $\Xi^0$ ,  $\bar{\Xi}^0$  which are assumed to be equally abundant. However, there is considerable isospin asymmetry in the decay pattern, and the branching ratio weight 0.77 arises as follows: 64% of  $\Lambda$  and 51.6% of  $\Sigma^+$  decay to protons. Statistical model evaluation shows that  $\Sigma^+$  (the only isospin channel decaying into  $p, \bar{p}$ ) are produced at the level of 25% of  $\Lambda + \Sigma^0$  (which one usually calls  $\Lambda$ ), considering within the statistical model that a significant fraction of all  $\Lambda$  originates in the  $\Sigma^*(1385)$  resonance.

Below the fit results we show the statistical parameters which are related to each fit. The results shown in the table 5 are obtained minimizing in the space of 3 parameters: the chemical freeze-out temperature  $T$ , and 2 chemical parameters  $\lambda_q, \gamma_s$ , the value of  $\gamma_q$  is set at its maximal value  $\gamma_q^2 = \gamma_q'^2 = e^{m_\pi/T}$  and the value of  $\lambda_s$  is derived from the strangeness conservation constraint. We note that even without this requirement the fit converges to local strangeness neutrality within a few percent.

In table 5 the last column presents the results of chemical equilibrium fit with 40% cascading. We note that several particle yields are not properly described and hence a large  $\chi^2$  results. However, on a logarithmic scale only results involving  $\Lambda, \bar{\Lambda}$  would be clearly visible as a discrepancy. The second and third last column show result of chemical non-equilibrium fit, the second last with 40% cascading which yields a good fit, and the third last with an increased 100% acceptance for the  $\Xi$ -cascading gives the smallest  $\chi^2$ , and has a very high confidence level.

Our current results, when compared to our earlier effort [43, 44] show a 7% reduction in the freeze-out temperature both for equilibrium and non-equilibrium case. Such lower  $T$  reduces selectively the relative yield of baryons. The required level of proton and hyperon yields are now reached at lower temperature due to the introduction of strange baryon weak cascading, or respectively, of experimental results which are corrected for

cascading. The range of temperature now seen agrees better with the expectations we had considering the effect of the fast expansion of QGP [50]. The chemical equilibrium freeze-out temperature,  $T = 164$  MeV, is in agreement with results of chemical equilibrium single freeze-out model of Broniowski and Florkowski [51, 52]. We believe that the case for single freeze-out particle production at RHIC will be statistically stronger with introduction of chemical non-equilibrium. We have seen this happen in section 5 for the SPS results.

Returning to discuss results seen in the bottom of table 5 we note that the specific strangeness content  $s/b \simeq 10$  in chemical non-equilibrium fits is 35% greater than the chemical equilibrium result. This originates in  $\gamma_s/\gamma_q \simeq 1.5$  (*i.e.*  $\gamma_s \simeq 2.5$ ). Figure 6 shows that the chemically equilibrated QGP phase-space has 10-14 pairs of strange quarks per baryon at  $1.062 < \lambda_q < 1.078$ . This implies that at RHIC-130 we have  $\gamma_s^{\text{QGP}} \simeq 0.85 \pm 0.15$ . This in turn *theoretically* implies that  $\gamma_s^{\text{HG}} \simeq 3(0.85 \pm 0.15) = 2.5 \pm 0.5$  given the enhancement of the HG phase space occupancy by a factor three seen in figure 7. Thus the specific yield of strangeness and strangeness occupancy we measure in the HG after hadronization is consistent with QGP properties with nearly saturated strangeness phase space. Even so, a further enhancement of  $\gamma_s$  can be expected in the 200 GeV RHIC run.

Once the comparison  $N$ - $N$  experimental results will become available, the enhancement of the production of multistrange baryons by this extraordinary strangeness abundance must exceed the high values seen at SPS by a factor  $(1.5-2.5)^{n_s}$ , where  $n_s$  is strangeness content of the hadron. An enhancement by a factor 50–300 of the  $\Xi$ ,  $\bar{\Xi}$ ,  $\Omega$ ,  $\bar{\Omega}$  yields is difficult to explain without new physics, and is natural for the fast hadronizing baryonpoor QGP phase.

In closing we would like to emphasize that the chemical non-equilibrium description of hadronization process is statistically highly favored at SPS and RHIC. Both the particle spectra and the HBT measurement of space-time size are favoring the sudden hadronization of a relatively small, short lived and rapidly expanding matter fireball, which reaction picture necessitates presence of chemical non-equilibrium. We hope that the reader who studies this report gains further the impression that a non-equilibrium chemical analysis of heavy-ion particle yields offers profound insight into the physical properties of the dense hadronic matter formed in the relativistic heavy-ion collisions.

## ACKNOWLEDGMENTS

Work supported in part by a grant from the U.S. Department of Energy, DE-FG03-95ER40937, and by NSF grant INT-0003184. Laboratoire de Physique Théorique et Hautes Energies, LPTHE, at University Paris 6 and 7 is supported by CNRS as Unité Mixte de Recherche, UMR7589.

## REFERENCES

1. R. Hagedorn. *Suppl. Nuovo Cimento*, **3**, 147, 1965.
2. R. Hagedorn and J. Ranft. *Suppl. Nuovo Cimento*, **6**, 169, 1968.

3. R. Hagedorn. Statistical bootstrap model. In *Cargese Lectures in Physics*, volume 5. Pergamon Press, Oxford, 1973.
4. E. Fermi. *Prog. Theor. Phys.*, **5**, 570, 1950.
5. J. Letessier, J. Rafelski, and A. Tounsi. *Phys. Lett. B*, **328**, 499, 1994.
6. A. Bialas. *Phys. Lett. B*, **466**, 301, 1999.
7. J. Rafelski, J. Letessier, and A. Tounsi. *Acta. Phys. Pol. B*, **27**, 1037, 1996.
8. D. Evans *et al.*, WA85 collaboration. *Nucl. Phys. A*, **566**, 225c, 1994.
9. D. Evans *et al.*, WA85 collaboration. In *Strangeness in Hadronic Matter: S'95*, p. 234, American Institute of Physics Proceedings Series, vol. **340**, New York, 1995.
10. D. Di Bari *et al.*, WA85 collaboration. *Nucl. Phys. A*, **590**, 307c, 1995.
11. S. Abatzis *et al.*, WA94 collaboration. *Phys. Lett. B*, **354**, 178, 1995.
12. T. Matsui and H. Satz. *Phys. Lett. B*, **178**, 416, 1986.
13. T. Matsui, B. Svetitsky, and L. D. McLerran. *Phys. Rev. D*, **34**, 783, 1986.
14. P. Braun-Munzinger, D. Magestro, K. Redlich, and J. Stachel. *Phys. Lett. B*, **518**, 41, 2001.
15. J. Letessier and J. Rafelski. *Phys. Rev. C*, **59**, 947, 1999.
16. J. Letessier, A. Tounsi, U. Heinz, J. Sollfrank, and J. Rafelski. *Phys. Rev. Lett.*, **70**, 3530, 1993.
17. J. Letessier, A. Tounsi, U. Heinz, J. Sollfrank, and J. Rafelski. *Phys. Rev. D*, **51**, 3408, 1995.
18. M. Gaździcki. *Z. Phys. C*, **66**, 659, 1995.
19. J. Rafelski, J. Letessier, and G. Torrieri. *Phys. Rev. C*, **64**, 54907, 2001.
20. I. Králik, *et al.*, WA97 collaboration. *Nucl. Phys. A*, **638**, 115, 1998.
21. C. Bormann, *et al.*, NA49 collaboration. *J. Phys. G*, **23**, 1817, 1997.
22. F. Siklér *et al.*, NA49 collaboration. *Nucl. Phys. A*, **661**, 45c, 1999.
23. P. G. Jones *et al.*, NA49 collaboration. *Nucl. Phys. A*, **610**, 188c, 1996.
24. H. Appelshäuser *et al.*, NA49 collaboration. *Phys. Rev. Lett.*, **82**, 2471, 1999.
25. S. V. Afanasev *et al.*, NA49 collaboration. *Phys. Lett. B*, **491**, 59, 2000.
26. J. Rafelski. *Phys. Rep.*, **88**, 331, 1982.
27. C. Greiner, P. Koch, and H. Stöcker. *Phys. Rev. Lett.*, **58**, 1825, 1987.
28. J. Rafelski. *Phys. Lett. B*, **190**, 167, 1987.
29. J. I. Kapusta and S. M. H. Wong. *Phys. Rev. Lett.*, **86**, 4251, 2001.
30. F. Becattini, M. Gaździcki, and J. Sollfrank. *Eur. Phys. J. C*, **5**, 143, 1998.
31. J. Letessier, J. Rafelski, and A. Tounsi. *Phys. Lett. B*, **410**, 315, 1997.
32. P. Braun-Munzinger, I. Heppe, and J. Stachel. *Phys. Lett. B*, **465**, 15, 1999.
33. P. Braun-Munzinger, J. Stachel, J. P. Wessels, and N. Xu. *Phys. Lett. B*, **365**, 1, 1996.
34. J. Letessier and J. Rafelski. *J. Phys. G*, **25**, 295, 1999.
35. J. Rafelski and J. Letessier. *Phys. Lett. B*, **469**, 12, 1999.
36. J. Rafelski and J. Letessier. *Acta Phys. Pol. B*, **30**, 3559, 1999.
37. J. Letessier, G. Torrieri, S. Hamieh, and J. Rafelski. *J. Phys. G*, **27**, 427, 2001.
38. G. Torrieri and J. Rafelski. *New J. Phys.*, **3**, 12, 2001.
39. F. Antinori *et al.*, WA97 collaboration. *Eur. Phys. J. C*, **14**, 633, 2000.
40. S. Kabana *et al.*, NA52 collaboration. *Nucl. Phys. A*, **661**, 370c, 1999.
41. S. Kabana *et al.*, NA52 collaboration. *J. Phys. G*, **25**, 217, 1999.
42. C. Markert, G. Torrieri, and J. Rafelski. Strange hadron resonances: Freeze-out probes in heavy-ion collisions. In this volume, 2002.
43. J. Rafelski. *J. Phys. G*, **28**, 1833, 2002.
44. J. Rafelski and J. Letessier. *Nucl. Phys. A*, **702**, 304, 2002.
45. C. Adcox *et al.*, PHENIX collaboration. *E-print nucl-ex/0204007*, 2002.
46. C. Adler *et al.*, STAR collaboration. *E-print nucl-ex/0203016*, 2002.
47. J. Castillo *et al.*, STAR collaboration. Mid-rapidity multi-strange baryon production at  $\sqrt{s_{NN}} = 130$  gev. In this volume, 2002.
48. C. Adcox *et al.*, PHENIX collaboration. *Phys. Rev. Lett.*, **88**, 242301, 2002.
49. July 2002 Presentations at Nantes. Quark matter 2002., Nuclear Physics A, 2003.
50. J. Rafelski and J. Letessier. *Phys. Rev. Lett.*, **85**, 4695, 2000.
51. W. Broniowski and W. Florkowski. *Phys. Rev. Lett.*, **87**, 272302, 2001.
52. W. Broniowski and W. Florkowski. *Phys. Rev. C*, **65**, 064905, 2002.